POLITECNICO
MILANO 1863

SCUOLA DI INGEGNERIA INDUSTRIALE
E DELL'INFORMAZIONE

Monte Carlo study of clinical treatment conditions provided by NOVAC 11 IOERT accelerator

TESI DI LAUREA MAGISTRALE IN
NUCLEAR ENGINEERING - INGEGNERIA NUCLEARE

Author: **Guglielmo Novelli**

Student ID: 967404

Advisor: Prof. Mario Mariani

Co-advisor: Dott. Gabriele Magugliani

Academic Year: 2021-22

Abstract

Nowadays radiotherapy techniques prove to be an excellent tool in the treatment of tumors. Among these, IOERT (Intra Operative Electron Radiotherapy Treatment) stands out, which involves the delivery of a beam of electrons through mobile linear accelerators. Through the latter it is possible to perform the treatment directly in the operating room, giving the possibility to use, in addition to the devices such as bolus and radiation protection vests, also radiation shielding disks. These latter have the task of protecting the healthy tissues posterior to the target.

The goal of this thesis is to perform a dosimetric characterization of clinical treatment conditions provided by the Novac-11 accelerator through a Monte Carlo approach. First of all, the Monte Carlo code was validated through the experimental measurements performed at the ASST Papa Giovanni XXIII (Bergamo) hospital in the context of the characterization of the Novac-11 LINAC for a delivery with a nominal energy of 10 MeV and with three different circular applicators of 10 cm, 6 cm and 5 cm in diameter.

Subsequently, the dosimetric variations induced by the presence of radiation shielding disks along the beam axis were studied. In particular, the two double-layer disks used at the ASST Papa Giovanni XXIII (Bergamo) hospital were studied: one in aluminum-lead, the other in PEEK-steel. The first one always saves at least 99% of the dose to healthy tissues but has an important backscattering phenomenon that can impose isodose regions higher than 105% of the prescribed dose. The second, on the contrary, has a much more modest backscattering phenomenon, which does not vary the clinical condition, but for superficial targets it is observed an attenuation of transmitted dose of just about 80%.

The effect of the presence of an applicator bolus was then studied. From a dosimetric point of view, its main effect is to impose a rigid translation of the dose profile to shallower depth.

Finally, the amount of dose that reaches the patient's skin surrounding the applicator was observed. This is approximately 2% -3% of the maximum dose delivered during treatment. The use of radiation protection vests saves the skin about 25% of the dose.

Keywords: IORT, Novac-11, Monte Carlo simulation, FLUKA, radiation shielding disk.

Estratto

Le tecniche radioterapiche si dimostrano oggigiorno un ottimo strumento nella cura dei tumori. Tra queste si distingue la IOERT (Intra Operative Electron Radiotherapy Treatment) che prevede l'erogazione di un fascio di elettroni attraverso acceleratori lineari mobili. Attraverso quest'ultimi è possibile eseguire il trattamento direttamente in sala operatoria, dando la possibilità di utilizzare, oltre che ai devices come il bolo per l'applicatore e i corpetti radioprotezionistici, anche i dischi sottocutanei di schermatura dalle radiazioni. Quest'ultimi hanno il compito di proteggere i tessuti sani sottostanti il target.

Obbiettivo di questa tesi è quello di eseguire una caratterizzazione dosimetrica delle condizioni cliniche di un trattamento eseguito con l'acceleratore lineare Novac-11 attraverso un approccio Monte Carlo. In primo luogo, si è validato il codice Monte Carlo attraverso le misure sperimentali eseguite presso l'ospedale ASST Papa Giovanni XXIII (Bergamo) nell'ambito della caratterizzazione del LINAC Novac-11 per un trattamento con un'energia nominale di 10 MeV e con tre differenti applicatori circolari da 10 cm, 6 cm e 5 cm di diametro. Successivamente si sono studiate le variazioni dosimetriche indotte dalla presenza dei dischi sottocutanei di schermatura dalle radiazioni lungo l'asse del fascio. In particolare si sono studiati i due dischi doppio strato utilizzati presso l'ospedale ASST Papa Giovanni XXIII (Bergamo): uno in alluminio-piombo, l'altro in PEEK-acciaio. Il primo risparmia sempre almeno il 99% della dose ai tessuti sani, ma presenta un importante fenomeno di backscattering che può imporre regioni di isodose superiori al 105% della dose prescritta. Il secondo, al contrario, presenta un fenomeno di backscattering molto più modesto, che non varia la condizione clinica, ma per target superficiali si osserva un'attenuazione della dose trasmessa di solo circa l'80%.

Si è poi studiato l'effetto della presenza del bolo per applicatore. Da un punto di vista dosimetrico l'effetto principale è quello di imporre una translazione rigida verso la superficie della curva di dose in profondità.

Infine, si è osservata la quantità di dose che giunge alla cute del paziente circostante l'applicatore. Questa è pari circa 2%-3% della dose massima erogata durante il trattamento. L'utilizzo dei corpetti radioprotezionistici risparmia alla cute circa il 25% di dose.

Parole chiave: IORT, Novac-11, simulazioni Monte Carlo, FLUKA, dischi sottocutanei di schermatura dalle radiazioni.

Contents

Chapter 1

Scope and structure of the work

Nowadays radiotherapy techniques have been established as therapies for the treatment of tumors. Radiotherapy makes use of ionizing radiation to affect the tumoral cells. Conventional radiotherapy is based on the irradiation of the tumor with an X-ray beam that transfers high energy to the tumoral cells, sterilizing the tumor and preventing a further increase of its mass. The aim of radiotherapy is to give dose to the tumor sparing the surrounding healthy tissues, even if sometimes it's not possible to achieve such goal.

One of the most recent radiotherapy techniques is Intra Operative Electron Radiotherapy (IOERT) which uses a beam of MeV electrons to treat semi-deep tumors in the range of a few centimeters [1]. The peculiarity of this treatment is that it can be performed directly in the operating room through mobile linear accelerators.

The purpose of this work is to observe, through Monte Carlo simulations performed with the FLUKA program, the variation of the dose curves in depth to the variation of the IOERT treatment set up performed with a NOVAC-11 accelerator. Indeed a IORT treatment allows the use of various devices that can influence the overall dose distribution. These devices are radiation shielding disks, radiation protection vests and applicator bolus.

First of all, it is necessary to validate the code, that is to find the simulation parameters that return a dose profile equal, within a certain error, to that of an experimental measurement performed under reference conditions. These are in fact easily reproduced with a phantom filled with water. The validation process is focused on treatments provided with a nominal energy of 10 MeV and with three different circular applicators of 10 cm, 6 cm and 5 cm in diameter.

The IOERT treatment, being performed in the operating room, gives the possibility to insert radiation shielding disks in order to protect any radiosensitive tissues. However,

backscattering phenomenon are expected to increase the dose in the area preceding the radiation shielding disks. These could be used to increase the treatment area, which is defined as the area that receives at least 90% of the prescribed dose. The experimental measurement of a set up that involves the use of radiation shielding disks is not easy. In fact, the set up to be implemented is very complex because it is necessary to arrange the disks in a water phantom; moreover it is necessary to repeat the measurement for a large number of times to take into account all the possible geometries. The power of the Monte Carlo approach therefore allows to reproduce this set up and to obtain a truthful result without having to irradiate directly with the accelerator.

Another interesting aspect that can be simulated is the amount of dose that reaches the skin surrounding the applicator during treatment. These are in fact made of PMMA (Poly Methyl Methacrylate) which allows leakage of primary and generation of secondary radiations. In particular, one of the goals is to reconstruct the energy spectrum of the electrons diffused through the applicator and that due to the Bremsstrahlung X-rays generated in the applicators. The outcomes of the experimental measurements are provided by the ASST Papa Giovanni XXIII (Bergamo).

IORT

EBRT (External Beam Radiotherapy) is the traditional radiotherapy treatment used to treat cancer. It involves the emission of targeted radiation beams from the outside of the body at various angles, generally through a linear accelerator (LINAC). The radiation emitted is generally X-rays, but it is also possible to use electrons or protons. The goal is to give an important dose to the CTV (Clinical Target Volume), trying to spare the surrounding healthy tissues. CTV indicates that region of volume, containing the tumor mass, that should receive the dose prescribed by the treatment. It is necessary to divide the treatment into several sessions in order to respect the dose restrictions imposed on healthy tissues. Generally a EBRT treatment involves a delivery of about 50 Gy in 25 sessions [1].

IORT (Intra Operative Radiotherapy Treatment) is a radiotherapy treatment performed with the aim of sterilizing the tumor bed, after surgical resection of the mass, to reduce the possible reoccurrence of local disease. In the case of neoplasms in an initial state, it can be used as a single treatment or combined with EBRT as a boost [1].

It is generally performed using an electron beam. In this case the treatment is called IOERT (Intra Operative Electron Radiotherapy Treatment). This treatment has the particular advantage of being able to be performed directly in the operating room through a mobile linear accelerator.

The treatment can also be performed using low-energy X-Rays emitted by a spherical applicator, which generates a homogeneous and isotropic flux. In this case the treatment is called kV-IORT.

From now on, IORT will refer to the IOERT treatment.

To perform an IORT treatment, however, it is also possible to use non-mobile accelerators (generally used for EBRT), but in this case it is necessary to set up the operating room directly in the radiotherapy bunker or transport the patient to the bunker following the surgery, increasing the complexity of the whole treatment [2].

The treatment is generally performed with an open wound such that it is necessary to obtain a "step" beam in order to give the right amount of dose to the tumor bed and spare the surrounding healthy tissues, which is why an electron beam is preferred. Indeed an electron beam guarantees a high dose to the target and to spare the surrounding healthy tissues. In fact, a treatment with electrons provides an irradiation field with the following characteristics:

- Sufficiently extended to cover the entire target (the dose in the target area must have a value equal to at least 90% of the prescribed dose [1])
- Modest penumbra (region in which the dose value, normalized to the maximum value, is between 20% and 80%)
- Low dose on the surface
- Rapid descent of the distal dose

Figure 1.1 shows the comparison between the PDD (Percentage Depth Dose curve), the percentage depth dose profile normalized with respect to the maximum value, of a monoenergetic electron beam and that of a photon beam in a sample of water at equal energy [3]. It is observed that the electron irradiation field useful for the treatment of the tumor, that is the region that has a value of at least 90% of the maximum dose, is very small, but has a much steeper penumbra. It follows that for the treatment of the same superficial tumor, the choice of a treatment with electrons allows to save considerably the healthy tissues posterior to the tumor.

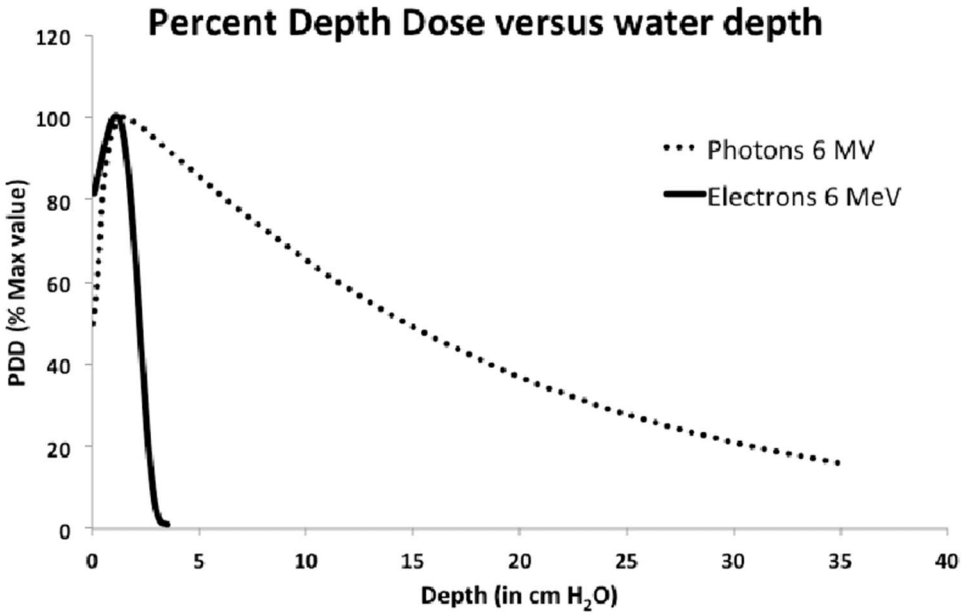

Figure 1.1 Comparison between the PDD of a 6 MeV electron beam and the one of a 6 MeV photons beam [3].

Historically, IORT treatment was indicated for rectal carcinoma, pancreatic neoplasms and peritoneal sarcomas [1, 4, 5]. It has also recently established itself in the treatment of breast cancer, on which this work is focused [4].

In the case of intra-operative treatment with an open wound, a dose of about 20-25 Gy, equivalent to a full cycle of conventional radiotherapy, is transferred to the tumor bed in a single session [1]. In the case of treatment as a boost, on the other hand, the dose is about 9-15 Gy [1].

NOVAC-11

Novac-11 (Sordina IORT Technologies S.p.A., fig. 3) is one of the mobile linear accelerators used for IORT treatment. It features a gantry that can be moved at various angles to allow it to be used in the operating room and to easily irradiate the target. This has the ability to perform both macro-movements for approaching the bed and micro-movements to facilitate alignment and the "docking" with the applicator.

It generates beams with four different nominal energies (from 4 MeV to 10 MeV).

The dose rate varies between 4 Gy / min and 30 Gy / min, with a dose per pulse between 7 mGy and 56 mGy.

The beam initially has a pencil beam geometry and is scattered on a thin titanium filter to obtain an adequate geometry. The beam is then collimated through an applicator positioned in "hard-docking" mode. The applicator consists of two PMMA tubes of which the first is fixed to the accelerator, the second is positioned directly on the target and subsequently, thanks to the micro-movements of the gantry, these are connected. The second applicator has a variable diameter between 3 cm and 10 cm in order to focus the beam on the target, sparing the surrounding healthy tissues. The collimation system imposes a source-skin distance (SSD) that varies between 50 cm and 120 cm.

Figure 1.2 Breast cancer treatment: positioning of the applicator and the bolus to avoid the phenomenon of tissue herniation. [1]

The applicator is placed in direct contact with the patient's skin. A possible phenomenon of tissue herniation is observed in the applicator, which generates a negative dosimetric effect. In particular, some areas of the skin will be in close contact with the applicator and other areas will be further away from it, with the possible generation of air cavities. There will be the possibility that more and less irradiated regions will be generated. The solution is the use of a bolus that allow to avoid herniation and to irradiate uniformly the entire surface of the target. The bolus generally consists of a polymeric material disk, a few millimeters thick and with a slightly larger surface than that of the applicator [6, 7].

Using this device is observed another benefit. Being made of polymeric material, a tissue-equivalent material, it will simply shift the PDD to the shallower depth, behaving like the first millimeters of the skin. By adjusting the thickness of the bolus it will therefore be possible to increase the dose on the surface of the target. This will in fact absorb that component of the superficial dose in which the PDD is less than 90%. The use of the bolus therefore allows to establish the reference geometric conditions of the treatment, thus being able to compare the dose distribution in a water phantom to that of the actual treatment.

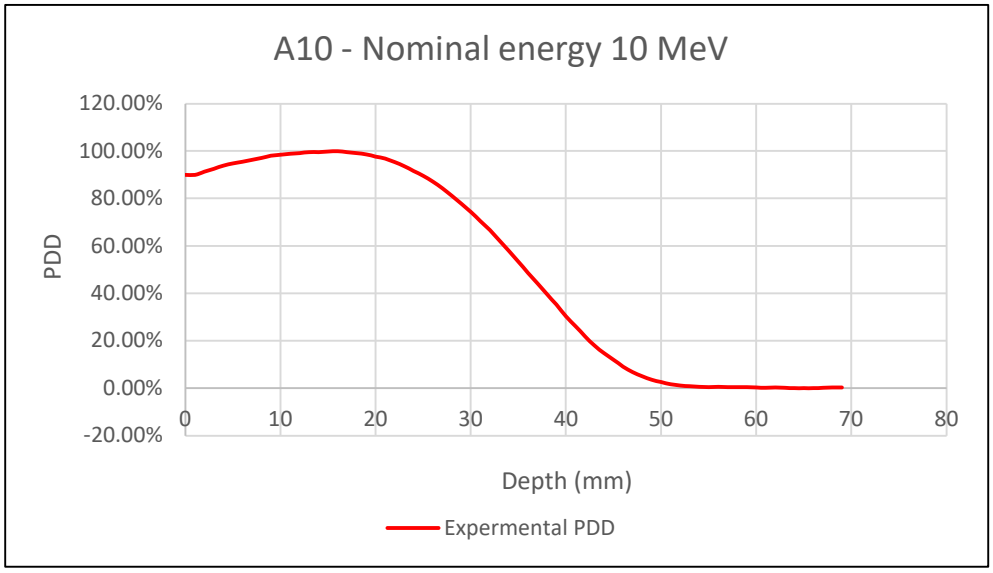

Figure 1.3 Experimental PDD for an irradiation with 10 MeV nominal energy and 10 cm circular applicator

The electron spectrum generated by the accelerator will not be mono-energetic but will also have a low-energy component. Firstly, since the pencil beam produced by the accelerator

already presents an energy spectrum ΔE in itself, then secondly the beam will undergo a further degradation phenomenon from both the titanium filter and the applicator. The interactions with these will also generate a X-rays bremsstrahlung component.

It is possible to apply subcutaneous radiation shielding disks to absorb the dose component below the isodose at 90%, saving the more radiosensitive tissues located deeper than the target. In general they have a diameter of 2 cm grater than that of the applicator used. In the case of breast treatment, the disks are placed posterior to the tumor bed to limit the dose to the lungs and rib cage. The use of disks saves healthy tissues up to 99% of the dose they would otherwise receive in their absence [8, 9]. Depending on the material they are made of, an increase in dose, even considerable, can be observed in the target region [8, 9, 10]. This is because the interaction of electrons with the disk can induce backscattering phenomenon, which become more probable as the Z of the material increases. However, the choice of high Z materials is mandatory in order to attenuate also the photonic component generated (mainly bremsstrahlung X-rays). Therefore the use of a dual material disk composed of two layers is necessary. The one placed deeper will have high density and high Z in order to attenuate as much as possible the unwanted radiation component. Another low-Z layer will then be placed above, generally either in aluminum or plastic material, to attenuate the backscattered component from the high Z layer and limit the dose increase in the target area. The simulations performed in this work and the experimental measurements obtained refer to a treatment performed with a Novac-11 accelerator. In particular, one of the objectives of this work is to observe how the PDD changes with the presence of radiation shielding disks through Monte Carlo simulation. In fact, the construction of an experimental set up for the measurement in this condition is complex, mainly because it is necessary to arrange the disks inside the water phantom and also because a large number of measurements are required.

IORT advantages

As part of the treatment of breast cancer, IORT is a replacement technique for EBRT and mastectomy as a post-operation treatment to avoid any relapses, with respect to which some advantages are observed [11].

Mastectomy, surgical removal of all or part of the breast, is an invasive surgical operation, which requires a medium to long-lasting recovery. On the contrary, radiotherapy treatments are non-invasive and provide for shorter recovery times.

EBRT, unlike the single intra-operative irradiation of IORT, instead provides a treatment lasting about 6 weeks, with 5 daily irradiations per week, which are added to the 6 months of chemotherapy already sustained by the patient [12, 13]. This additional period of treatment may in some cases lead the patient to prefer mastectomy to EBRT [12, 13].

In addition, there is a logistical problem: the patient's possibility of being able to reach the radiotherapy center. From an American study it was observed that the percentage of patients

Figure 1.4 Novac11 linear accelerator

who underwent radiotherapy treatment was 82% if the distance to travel was less than 10 miles, on the contrary, the percentage dropped to 42% if the distance to travel was greater than 100 miles [12, 13].

In addition to these social problems, the IORT treatment provides the following technical advantages compared to EBRT [11, 14, 15]:

- Direct visualization of the field to be irradiated, which allows a better delimitation of the volume to be treated [1]. The IORT treatment is therefore generally less radiotoxic.
- Homogeneous distribution of the dose.
- Possibility of being able to protect adjacent organs through the use of radiation shielding disks and by physical separation.
- Possibility to directly and actively control the volume to be irradiated. For example, graduated needles are used to measure the depth of the volume to be irradiated.
- Easy control of the total dose delivered.
- The administration of the treatment during surgery prevents the repopulation of neoplastic cell clones in the interval between surgery and EBRT, with a radiobiological advantage [11].
- The duration of irradiation is about 1-2 minutes.

IORT toxicity is generally related to the dose and type of anatomical structures involved in the treated volume and has mainly late effects [16, 17]. These increase when the prescribed dose exceeds 25 Gy [18].

Finally, the workload of the radiotherapy center is reduced, with a consequent reduction in the waiting lists for conventional radiotherapy. Moreover, it has been observed that as the time between tumor removal and the start of radiotherapy increases, the possibility of local control of the tumor decreases. It has been observed an increase of 1.1% in the absolute risk of local recurrence for each month of delay for breast cancer treatment [12, 25]. It is therefore essential that the treatment is carried out with the correct timing.

Treatment

The size of the tumor bed imposes the choice of nominal energy, since this determines the maximum depth at which the dose will be transferred, and the size of the applicator, which allows an adequate irradiation surface of the beam. The surface of the front view will have to consider the actual size of the tumor and a surrounding region, called the quadrant, where the possibility of recurrence is high. The maximum depth that has to be irradiated can be evaluated through direct methods, such as the use of graduated needles, or indirect imaging, such as CT [1].

The dose prescribed for an exclusive treatment is about 21 Gy at the 90% isodose[19], on the contrary for the boost treatment it is about 10 Gy at the 90% isodose[19]. The 90% isodose should be define in such a way that the entire clinical target volume is irradiated with at least 90% of the prescribed dose.

As already mentioned, the nominal energy of the beam is chosen in such a way as to reach the maximum depth required. In the most of cases, however, for convenience, it is possible to set the maximum nominal energy (10 MeV) and then screen the underlying healthy tissues with the radiation shielding disks. In this case, however, it will be necessary to consider the contribution of any back-scattering effect of the disks in order to limit the dose in the planning target volume below an isodose value of 105%, which is regarded as an acceptable lever of overexposure.

Physical aspects of IORT

One of the most complex aspects of IORT is the dosimetry of the treatment [21, 22, 23, 24]. This is because, unlike EBRT, IORT presents much higher dose rates, the geometry of the planning target volume is not chosen a priori but directly in the operating room and finally the presence of radiation shielding disks can change the amount of dose released due to the contribution of the back-scattering effect. Another aspect that differentiates IOERT from EBRT is the use of specific applicators: as mentioned, these are made of plastic material (generally PMMA) and

generally have a circular section. For specific applications, however, they can present other geometries, for example square or triangular. In addition, circular section applicators may have an oblique terminal part, i.e. angled with respect to the geometric axis of the beam (with angles between 15 ° and 45 °). Compared to a standard collimated beam, this type of applicator involves an increase in the diffuse component of electrons in the radiation field, with a consequent widening of both the energy spectrum and the angular distribution of the beam [25]. The diffuse component in a conventional treatment that uses electrons has a dose contribution of about 10% to the depth of the maximum dose (R_{max}), while in IORT this contribution can reach 40% [22, 26, 27, 28, 29, 30].

Of course, the degradation of the electron spectrum of a purely monoenergetic electron beam involves a modification of the dose curve in depth along the beam axis compared to standard collimation. In general a greater contribution at the surface, a lower R_{max} and a decrease in the amount of dose at depth is observed [26].

Another aspect that can change the trends of the dose curves in depth is the integrity of the applicators: even a small change in their physical or geometric characteristics (cracks, distortions, etc.) could change the dose curve in depth [1].

The different characteristics in terms of energy distribution and angle of the IOERT beams with respect to EBRT change the dosimetric parameters. These, especially for those detectors with dependence of the response on energy and angle, are difficult to evaluate. In addition, the high intensity and frequency of the pulses delivered limits the use of ionization chambers due to ion recombination phenomena, underestimating the dose by up to 40% [1].

Corrective factors for ionic recombination k_s are used to correct the measurement of ionization chambers [30, 31, 32, 33, 34, 35]. These are semi-empirical functional relationships as a function of the dose per pulse and the characteristics of the ionization chamber used. They are calculated by comparing the dose value obtained with the specific ionization chamber and a dosimetric method independent of the dose per pulse (generally radiochemical dosimeters such as Fricke or alanine dosimeters or solid-state dosimeters).

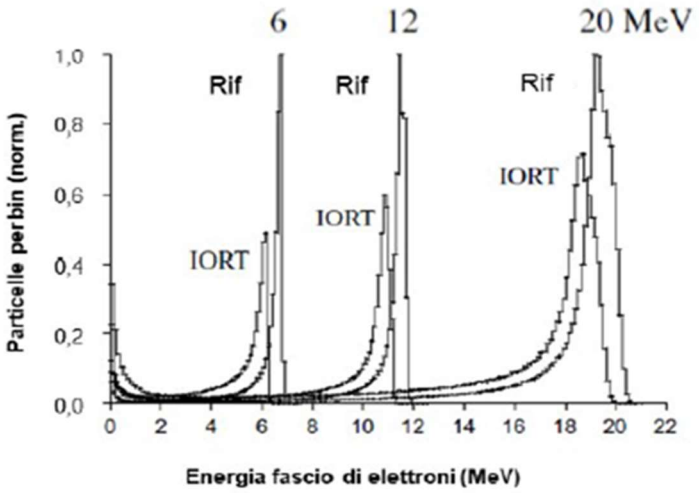

Figure 1.5 Comparison between the electron energy distributions at the phantom surface for the reference radiation field 10x10 cm2 and the IORT radiation field with diameter 9 cm for electron beams with nominal energy 6, 12 and 20 MeV [1]

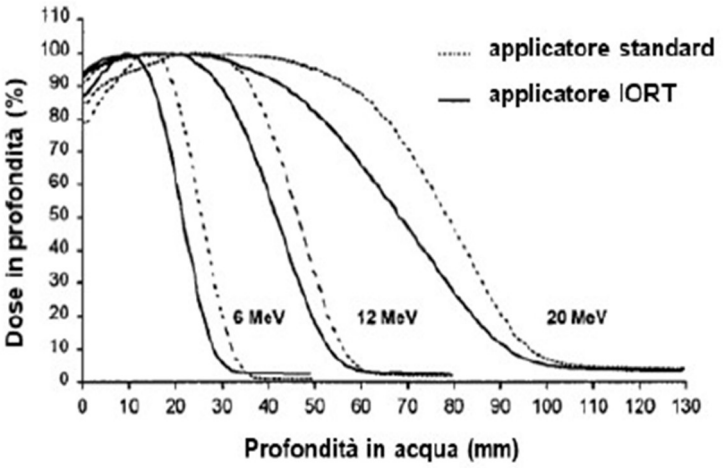

Figure 1.6 Comparison of the depth dose curves on the beam axis for IORT applicators with the curve obtained for the conventional beam (standard applicator 10x10 cm2). The nominal energies of the electron beams are 6, 12 and 20 MeV.[1]

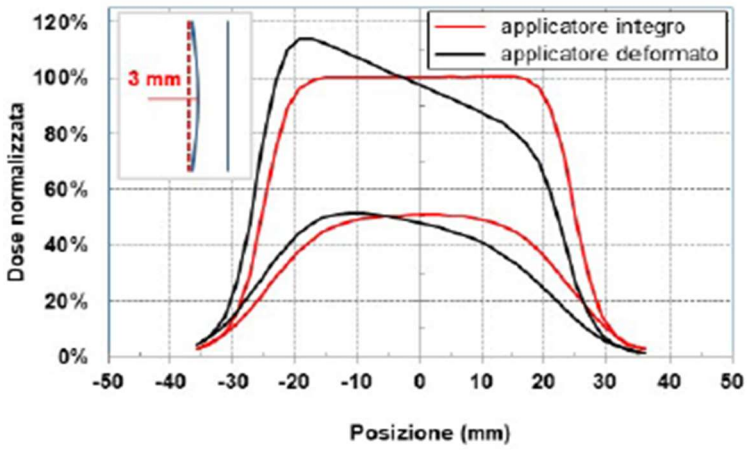

Figure 1.7 Comparison between the transversal dose profiles at depth Zmax and R50 of an intact flat applicator and of a deformed flat applicator evaluated at the maximum energy of a Novac-7 accelerator [1]

Dosimetry in reference conditions

It is necessary to identify reference conditions in order to be able to perform a dose measurement that is as independent as possible both from the spectrum emitted by the accelerator and from the chosen detector. Dosimetry under reference conditions allows to determine the absorbed dose in water with comparable accuracy with respect to other LINACs. There are various international protocols that can be used, for this work it was decided to follow that of the International Atomic Energy Agency (IAEA): the TRS 398 *"Absorbed Dose Determination in External Beam Radiotherapy: An International Code of Practice for Dosimetry based on Standards of Absorbed Dose to Water"* [36].

The Protocol provides for dose measurements under the following conditions:

- Phantom filled with water with a volume such that for each direction perpendicular to the beam axis it extends at least 5 cm beyond the largest dimension of the field at the depth at which it is measured. The phantom is made of plastic material with a thickness between 0.2 cm and 0.5 cm.
- Applicator with square section 10x10 cm or, alternatively, circular with a diameter of 10 cm. In both cases the applicator end must be flat.

- SSD (source-skin distance) of 100 cm. If it is not possible to obtain this SSD, use the lenght of the applicator. SSD is defined as the distance between the source and the skin of the patient. In IORT treatment is generally equal to the length of the applicator.
- The measurement is performed at depth Z_{ref}, where:

$$Z_{ref} = 0.6 * R_{50} - 0.1 \ [g / cm^2] \quad (1.1)$$

This depth is very similar to the depth at which the maximum dose transfer is observed but varies slightly with the variation of the energy and spectrum of the beam. The definition of Z_{ref} considerably reduces the dependence of the measurement on the type of detector chosen.
The absorbed dose measured in reference conditions will be calculated as

$$D_{w,Q} = M_Q * N_{D,w,Q0} * k_{Q,Q0} \quad (1.2)$$

Where:

- $D_{w,Q}$ is the absorbed dose at the reference depth Z_{ref} in water of an electron beam of quality Q and in the absence of the chamber.
- M_Q is the reading of the dosimeter corrected for the influence quantities temperature and pressure, electrometer calibration, polarity effect and ion recombination.
- $N_{D,w,Q0}$ is the calibration factor in terms of absorbed dose to water for the dosimeter at the reference quality Q_0.
- $k_{Q,Q0}$ is a chamber-specific factor which corrects for differences between the reference beam quality Q_0 and the actual beam quality Q.

Dosimetry in non-reference conditions

Dosimetry in non-reference conditions has as its purpose the experimental dosimetric characterization of radiation beams. For this reason, it is also generally called clinical

dosimetry or dosimetry under conditions of use. Characterization includes the following measures:

- The percentage depth dose curve (PDD) measured along the clinical axis of the beam. The curve is obtained from the ratio between the dose in depth and the maximum measured dose at depth R_{max}. The main parameters of this must then be indicated: R_{max}, R_{30}, R_{50}, R_{90} (i.e., the depths at which the dose is respectively maximum, at 30%, 50% and 90%), surface dose and percentage of dose due to the photon contamination of the beam resulting from the bremsstrahlung tail.
- The transverse profiles of dose in water, measured along two directions orthogonal to each other at the depths R_{max}, R_{30}, R_{50}, R_{90}.
- The isodose curves in water on the two main orthogonal planes containing the clinical axis of the beam, reconstructed starting from the PDDs and the measured transversal dose profiles.

Dosimetric characterization must be performed for each applicator, for each energy and for each SSD in clinical condition.

Furthermore, for each single applicator it is necessary to calculate the value of the Output Factor (OF) parameter. The OF parameter of an applicator is described by the ratio between the dose in water measured at R_{max} with this applicator and the dose in water measured at R_{max} with the reference applicator (circular applicator with a diameter of 10 cm). This parameter must be measured for each applicator, at each energy and SSD of clinical use, at the irradiation conditions as similar as possible to those of the treatment. It is important to characterize each individual applicator since, as already discussed, the amount of radiation diffused in the beam varies according to the geometry and length of the applicator and is responsible for the degradation of the energy spectrum of the beam. OF parameters values are generally greater than 1 since beam degradation due to smaller applicators leads to greater surface dose deposition [1].

Determination of deep dose

The determination of the dose in depth is performed by irradiating a phantom filled with water and with walls in plastic material under the treatment conditions. Inside the phantom there is a motorized system that allows movement along the clinical axis of the detector during irradiation, in order to obtain dose distribution in depth. The motorized system must ensure accuracy and reproducibility of positioning of the detector of 0.1 mm.
The same motorized system allows the transversal movement across the beam axis for the measurement of transversal profiles.
In this work a PTW microdiamond detector was chosen as the dosimeter. This dosimeter is a solid-state detector consisting of a single synthetic diamond crystal. It has the following features [26, 37]:

- A high spatial resolution that allows a precise measurement of the penumbra in small fields.
- A very small sensitive volume, down to 0.004 mm^3.
- An almost independent response from the angle of incidence of the radiation.
- It is considered perfectly water-equivalent.
- Linear response with dose.
- Response independent of both energy and dose rate, useful for the very high dose per pulse of Novac-11.
- Fast response on time.
- Energy necessary for the promotion of the electron from the valence band to that of conduction 13 eV. It is possible to do dosimetry with electron beams that have energies in the 6-20 MeV range.

Chapter 2

Monte Carlo method

The Monte Carlo method exploits a computational approach based on random sampling to obtain approximate numerical results of mathematical problems which, having many degrees of freedom, cannot be solved analytically. In particular, the Monte Carlo method refers to a family of methods used to approach problems of various nature through simulations. These always have the same approach:

- Definition of the input domain and its probability density.
- Generation of a random input through various sampling methods.
- Execution of a cycle of simulations through a stochastic model.
- Mediation of the results of the single simulations to obtain an expectation value of the system.
- Estimation of the statistical error (variance).
- Applications of variance reduction techniques (if necessary).

The applications are various and concern many fields of medical physics such as: radiological diagnostics, radiotherapy, nuclear medicine and radiation protection [38, 39, 40].
The physics of ionizing radiation deals with a wide range of particles (in radiotherapy, mainly photons, protons, electrons, light ions are used) and each of these gives rise to a more or less complex cascade of events in the matter. Monte Carlo simulations in this area therefore require a large amount of information both on the properties of the particle and of the matter in which the interaction takes place. In the case of simulation of indirectly ionizing particles, it is possible to use an event-by-event approach since the interaction occurs mainly only by scattering [41]. On the contrary, in the case of directly ionizing radiations, and in particular for electrons, this approach becomes too expensive from a computational point of view since, in

addition to the energy losses due to scattering, it is also necessary to consider the electromagnetic interaction between particle and matter. Consider that, with the same amount of energy lost, an electron will interact approximately 10^5 times more than a photon [41]. A condensed history method is therefore generally used. In a condensed history method the cumulative effects of multiple electron collisions are approximated in a single "step" of the path length specified by the user [41].

The application of the Monte Carlo method in the field of particle physics is essentially based on the simulation of the transport of the primary particles, i.e. the electron produced by the accelerator, and the events generated by them for the determination of observables which cannot generally be obtained analytically.

One of the advantages of using the Monte Carlo method in medical physics is the possibility of studying the variation of the output of a system with respect to the setup of the analyzed problem without having to perform an experimental measurement with the modified set up. In order to do this it is necessary to preliminarily validate the code. Validation is the process in which, starting from an experimental measurement, the parameters of the simulation that allow to obtain an output which is, within a certain error, equal to the experimental measurement are found. In this work, as explained in the next chapter, the validation concerned the determination of the energy spectrum of the electrons produced by the Novac-11 accelerator, ie the input domain and the probability density of this, with the goal of reproducing the dose deposition profile obtained experimentally under reference condition.

After such code validation it was observed how the dose distribution in a water phantom varied in the case of the introduction of radiation shielding disks posterior to the region corresponding to the therapeutic target and the effect of other devices.

The simulations were performed through the Monte Carlo code FLUKA (version mainly used: FLUKA 2021.2.6) [42] and the graphical interface flair [42].

Monte Carlo method's history

The Monte Carlo method falls within the branch of experimental mathematics. In fact, an inductive approach is used to reach the conclusion, based on the repetition of an experiment. Historically, the first application of the Monte Carlo method is attributed to the Comte de Buffon experiment (1733). The problem is the following: given a space where there are a series of parallel and equidistant lines at a distance D, what is the probability that by dropping a needle of length L it will touch a line?

The probability will be equal to $p = \frac{2L}{\pi D}$

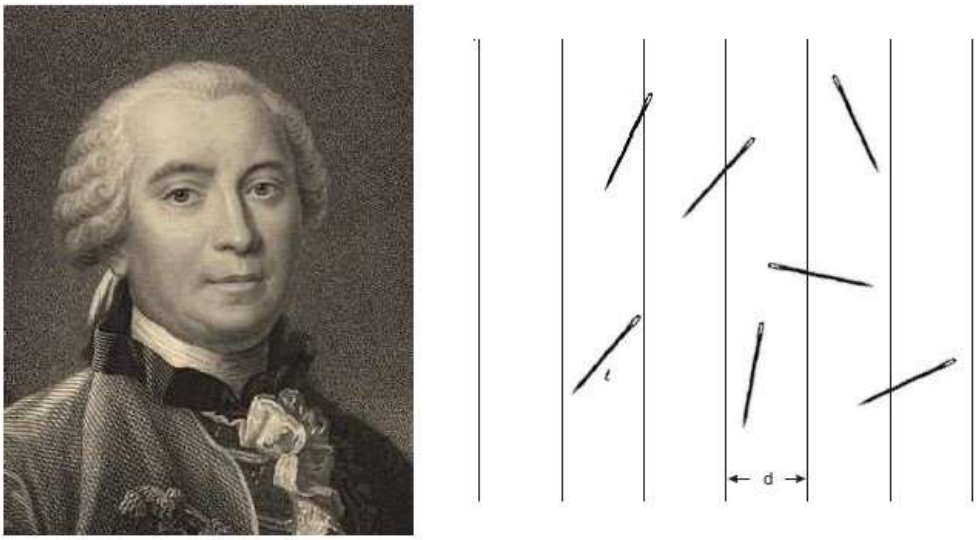

Figure 2.1 Comte de Buffon and the problem's representation

However, the probability can be exploited to obtain an estimation of π. In fact, by performing *N* repetitions of the experiment and counting the *n* times a needle touches a line, it's possible to rewrite the probability as:

$$p = \frac{n}{N} = \frac{2L}{\pi D} \rightarrow \pi \sim \frac{2LN}{Dn} = \frac{2Lp}{D} \tag{2.1}$$

100,000 repetitions are required to obtain an approximation of π to the second decimal digit. Convergence is slow, but the method works.

The first modern use of the Monte Carlo method is to be attributed to Enrico Fermi, John von Neumann and Stanislaw Ulam who, in the context of the Manhattan project (1940), exploited computational methods of random sampling to solve the complex integral present in the neutron transport theory [43].

The term "Monte Carlo method" was coined only later by Nicholas Constantine Metropolis referring to the well-known casino (1950) [43].

The method

In general, Monte Carlo methods can be applied to both deterministic and probabilistic problems. In the first case a stochastic model is proposed whose average value coincides with the original solution of the problem. Radiation-matter interaction, the subject of this work, is of probabilistic nature and therefore its mathematical treatment can be used directly as a stochastic model for simulation.

The goal of a Monte Carlo simulation is to find an output value Ω of the studied system. This will be obtained through a simulation of the stochastic model starting from a random input belonging to a previously described domain and sampled according to the probability density that describes the domain itself. There are various sampling methods, in this work the "rejection sampling" was used, which will be explained later.

Given a stochastic model, let Ω be the output value to be determined. Executing a cycle of N simulations, N random variables X_i are obtained, such that Ω is the expected value of each of them. Therefore as an estimator of Ω it's possible to take the arithmetic mean X of the N random variables obtained from the N simulations.

$$X = \frac{\sum_{i=1}^{N} X_i}{N} \tag{2.2}$$

Each of these random variables X_i will have an expected value $E[X_i] = \Omega$ and a variance $var[X_i] = \sigma^2$.

$$E[X] = \frac{\sum_{i=1}^{N} E[X_i]}{N} = \Omega \tag{2.3}$$

X is defined as an undistorted estimator of Ω as it has an expected value equal to the output value to be determined.

To determine the sensitivity of the estimator X towards the output value Ω it is necessary to study the variance of X. This can be calculated using the Bienaymé formula:

$$Var(X) = E[(X - \Omega)^2] = Var\left[\frac{\sum_{i=1}^{N} X_i}{N}\right] = \frac{\sum_{i=1}^{N} Var(X_i)}{N^2} = \frac{\sigma^2}{N} \tag{2.4}$$

The variance is a statistical indicator of the dispersion of the values of a variable around the mean value. It follows that the smaller the variance, the more the values of the variable will be concentrated around the mean value. By imposing a tolerance and estimating σ^2 it will be possible to obtain the number N of simulations necessary to reach the desired sensitivity of the estimator X.

However, it must be emphasized that as the number of simulations increases, and therefore the sensitivity of the estimator X, the computational time of the simulation cycle will increase accordingly. It will therefore be necessary to find a compromise between estimator sensitivity and computational time.

To demonstrate the fact that as the number N of simulations increases, the estimator X will tend to converge to the output value Ω, the "law of large numbers" and the "central limit theorem" are quickly introduced. The former states that, having a large enough number of independent variables with the same mean μ and the same standard deviation σ, they will tend to distribute following a normal distribution. It follows that:

$$\lim_{n\to\infty} P\left(\frac{X_1 + X_2 + \cdots + X_n - n\mu}{\sigma\sqrt{n}} \leq x\right) = \Phi(x) \tag{2.5}$$

The "central limit theorem" states instead that, having a large enough number of independent variables with the same mean μ and the same standard deviation σ, it's possible to construct the variable Z defined as:

$$Z = \frac{X - \mu}{\frac{\sigma}{\sqrt{n}}} \tag{2.6}$$

Which will be distributed as a unit normal random variable *N(0,1)*.

If a variable $z\alpha$ is introduced for which α is a number between 0 e 1 and such that, for a unit normal variable, you get that $P(Z > z\alpha) = \alpha$. Then rearranging the two theorems the following result is obtained:

$$P\left\{X - \frac{z\left(\frac{\alpha}{2}\right)\sigma}{\sqrt{n}} < \mu < X + \frac{z\left(\frac{\alpha}{2}\right)\sigma}{\sqrt{n}}\right\} = 1 - \alpha \tag{2.7}$$

So it can be said that the probability that the mean μ is included in the indicated range is $1 - \alpha$.

For a Monte Carlo simulation, the mean μ will be equal to the output value Ω and X will be the estimator. Set a probability $1 - \alpha$, it's possible to derive the minimum number of simulations necessary to fall within the desired confidence interval.

Finally, to estimate the variance the "empirical variance" can be used:

$$s^2 = \frac{1}{N-1}\sum_{i=1}^{N}[X_i - E(X_N)]^2 \tag{2.8}$$

If N is big enough, at least 100, $s^2 \rightarrow \sigma^2$.

Random variable generation

Any Monte Carlo method involves the generation of a series of random inputs sampled through the probability density (PdF) that describe the domains. If the probability density is easily sampled, such as a uniform density or a Gaussian, this can be sampled directly. Otherwise the input generation process includes:

- The generation of a sequence of random numbers, typically included in the interval [0, 1].
- Using an inversion method to switch from the sequence of random numbers to the probability density of the data set to sample.
- Sampling the domain of the input set.

The generation of the sequence of random numbers included in the interval [0, 1] takes place through mathematical algorithms. In reality, since the sequence is typically generated through

deterministic algorithms, a totally random distribution is not obtained. Therefore, it's better to refer to pseudo-random distributions.

As an example, one of the simplest and most ancient algorithms of generation of pseudo-random numbers is cited: the "linear congruential generator" (LCG). This consists of the following discontinuous piecewise linear equation:

$$X_{n+1} = (aX_n + c)\ mod\ m \tag{2.9}$$

Where:

- X is the generated sequence
- m is a positive number called "modulus"
- a is a positive number such that $0 < a < m$ called "multiplier"
- c is a positive number such that $0 \leq c < m$ called "increment"
- X_0 is a positive number such that $0 \leq X_0 < m$ called "seed"
- *mod* is the modulus function that returns as a result the remainder of the division by the preceding and consequent numbers -> it returns the remainder of $\frac{(aX_n+c)}{m}$

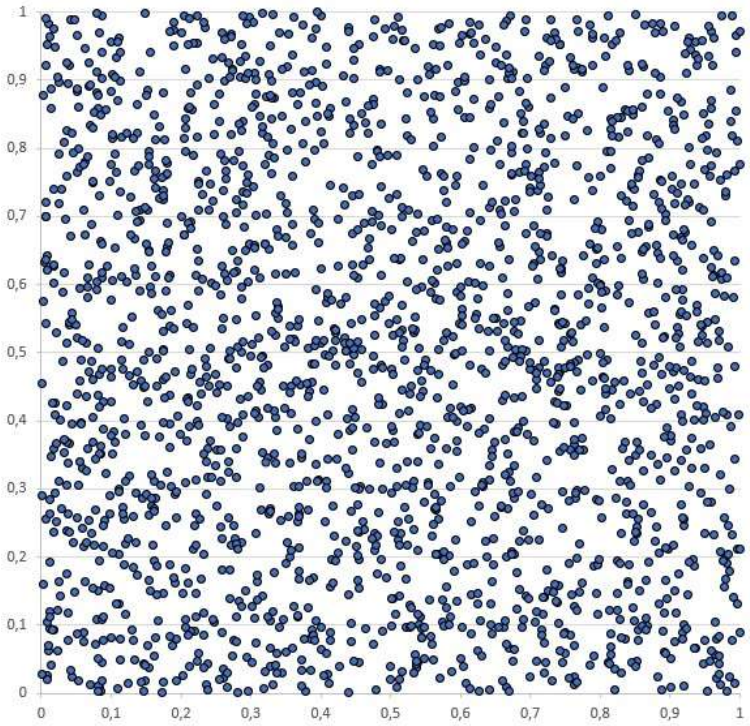

Figure 2.2 Example of a Random generation of points between 0 and 1 obtained plotting 1000 random numbers generated by Excel

There are other "versions" of this algorithm. For example, if the increase is zero, the algorithm is called "multiplicative congruential generator" (MCG).

As said initially this kind of distributions is call pseudo-causal distributions since by choosing the same initial parameters (a, c, m, X_0) the same sequence of random numbers is always obtained.

In general, any random number generator must have the following characteristics:

- Absence of apparent correlation between the numbers of the sequence.
- Uniform distribution of the random numbers obtained.
- High calculation speed of the algorithm.
- Period between [0, 1].
- Sufficiently long sequence period.

After obtaining a sequence of random numbers it's necessary to correlate it to the PdF of the data set to be simulated. There are various techniques, the one used in this work is the "rejection sampling". The idea is to start from a known PdF, such as a uniform or Gaussian density, which can be easily sampled and exploit this to sample the unknown PdF. For example, choose a uniform density $g(x)$ with domain equal to the PdF to be sampled $f(x)$ and find a constant C such that $C \geq \frac{f(x)}{g(x)}$ fo each x belonging to the domain.

The domain is then expressed as $x = X(x_{max} - x_{min}) + x_{min}$ where X is a random value in the interval [0,1] calculated through an algorithm, while x_{max} and x_{min} are the minimum and maximum value of the domain of the two PdF.

By generating a first random number, it's possible to identify a point in the domain x_0. Generating a second random number h instead:

- x_0 is accepted and can be used as an input if $h * C * g(x_0) \leq f(x_0)$.
- On the contrary, x_0 is rejected if $h * C * g(x_0) > f(x_0)$.

By repeating this procedure iteratively, it is possible to sample a set of inputs described by any PdF, even not normalized.

It should be noted that to reduce the sampling time of the process it is important to choose C such that $C * g(x_0) = f(x_0) + \delta$ where x_0 is the point where $f(x)$ has tha maximum value and δ is an infinitesimal.

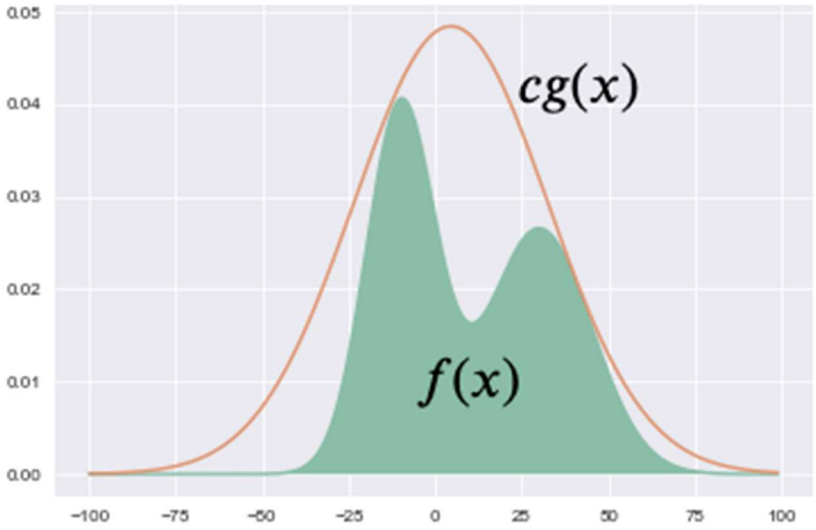

Figure 2.3 Representation of Rejection Sampling method

Monte Carlo codes for medical radiation physics

In the introductory paragraph, the potential of using Monte Carlo methods in the field of medical physics was highlighted.

Over time various general purpose Monte Carlo suites have been developed for the study of high energy physics. These were subsequently exploited also in the field of medic physics. Some are mentioned [38]:

- EGS4 (Electron Gamma Shower) [44] is used for simulation of coupled electron-photon transport in arbitrary geometry. It presents an energy range of applicability of 1keV-1GeV. [Stanford Linear Accelerator Center SLAC, USA]
- MNCP [45] is used for neutron, photon and electron simulations. It has been successfully used in the field of medical physic, for example to calculate the bremsstrahlung spectra from medical linear accelerators or to evaluate the dose

distributions around brachytherapy sources. MCNP has also been used for radioimmunotherapy and Boron Neutron Capture Therapy applications. [Los Alamos National Laboratory LANL, USA]

- GEANT4 [46] is able to manage electrons, positrons, hadrons, γ- and x-rays and muon interaction. It is used in particular for particle cancer treatment such as hadrontherapy and Boron Neutron Capture Therapy. [Conseil Européen pour la Recherche Nucléaire CERN, Europe]
- PENELOPE [47] is used for simulation of coupled electron-photon transport in arbitrary materials with an energy range of applicability from some keV to about 1 GeV. The particularity of this code is that the electron histories are generated with a mixed procedure, which combines detailed simulation of hard events with condensed simulation of soft interactions. [University of Barcelona, Europe]
- FLUKA [42] is able to simulate most of the particles over an extended energy range (1 keV-10^{13} keV). It is also able to build complex geometries. It is the code used in this work and it will be illustrated better in the next paragraph. [CERN/Istituto Nazionale Fisica Nucleare INFN, Europe]

FLUKA history

FLUKA, acronym of FLUktuierende KAskade, is a general-purpose Monte Carlo code for the simulation of radiation-matter interaction phenomena.

The first version of FLUKA was written by Johannes Ranft between 1962 and 1967 while he was working on the phenomenon of hadronic cascade at CERN [42].

From the 1960s the code was implemented several times, always under his supervision. Three "generations" of the code can be recognized:

- The first "generation" (1962-1978), of which the main authors are J.Ranft and J.Routti, was mainly exploited to design shielding of high energy proton accelerators and to evaluate the performance of NaI crystals used as hadron calorimeters. As mentioned, this first version was designed to simulate the phenomenon of hadronic cascade [42].

It was able to simulate charged protons, neutrons and pions. The outputs that could be obtained were only star density and the energy deposited. A 50 MeV transport cut off was set for any particle and the phenomena of low energy particle transport and electromagnetic cascade were not simulated but sampled by “typical space distributions”.

- The second "generation" (1978-1988) provides a total re-design of the code in order to introduce a modern formulation of the hadronic interaction and a new parameterization of the electromagnetic cascade. The project, always under the supervision of J.Ranft, is carried out through various collaborations. One of the most important implementations was that concerning the description of geometry, with the introduction of Cartesian and spherical geometries and the possibility of working with complex composite materials [42].
- The third "generation" (1988-present) had as its main objective that of being able to manage hadrons with higher energies, in the order of several TeVs, for simulations concerning the shielding of new generation accelerators. The previous structures, however, had various limitations, in particular they are not able to simulate the effect of the presence of large magnetic fields, the deposition of energy in very small volumes, the interaction of low-energy neutrons, etc.

  Ferrari and A. Fassò, the main authors of this last generation, set themselves the goal of transforming the old versions of Fluka into a code capable of simulating most of the particles and their interactions with most of materials and in a wider energy range (1keV - hundreds of TeV). In about six years they achieved the goal of transforming FLUKA into a general-purpose Monte Carlo code for the simulation of radiation-matter interaction phenomena [42].

FLUKA input

The FLUKA input file is an ASCII text with the '.inp' extension. The file has a variable number of commands, consisting of one or more CARDS. Each CARD consists of an SDUM, a character

string, and various numerical values known as WHATs. Some WHATs represent numerical quantities, while others are indices corresponding to a material, a type of particle, a region etc. In this last case, it is possible to replace the number by the corresponding name (a character string).

FLUKA has a working principle very similar to most Monte Carlo software for the simulation of the interaction between radiation and matter. The following items can generally be recognized in the input file [42]:

- Title and comment of the simulation.
- Source radiation. The description of the source includes the type of primary particle, its energy, its position and the direction vector of emission.
- Geometry. FLUKA uses a combinatorial geometry approach to construct the geometry of the bodies making up the simulation environment. Various geometries can be defined (planes, cylinders, parallelograms, etc.) which will be connected through Boolean operations to describe regions, which identify a portion of space characterized by a single material.
- Materials. Once the regions have been implemented, it will be necessary to attribute the material they are made of. There is a predefined set of materials, but any material can be added by specifying density and elemental composition. In the case of simulations with neutrons, it is also important to specify the isotope of the element and its cross-sectional value.

  Finally, a region is always defined that delimits the boundaries of the problem, to which the material BLCKHOLE (black hole) is attributed. This is used by the code to end the transport of any particles that reach this region.
- Transport parameters. Once the source and the geometry of the problem have been described, it is possible to modify a series of parameters that increase or reduce the precision of the simulation, varying the computational time. As an example the follower parameters are cited: cut off transport energy, step size, physical events not simulated by default, particles not to be transported, etc.

There are default settings options designed for simulating specific cases such as calorimetry, dosimetry or shielding problems.

Of course, parameters can be set for specific problems. However, it is important to underline that the inappropriate choice of some trasport parameters can lead to a non-physical result of the simulation.

- Simulation parameters. In order to be able to perform the simulation, it is necessary to choose the number of primaries to be simulated, as these increase both the precision of the simulation and the computational time required. By setting a desired maximum statistical error, the number of primaries will instead be a consequence of the chosen error.
- The seed of the random number generation algorithm must then be chosen in order to obtain statistically independent results from time to time.
- Scoring. It is possible to simulate various physical quantities, such as: dose, kerma, fluence, etc.

  In order to obtain these quantities, it is necessary to set up a geometric mesh, independent of the previously described regions, which identifies the voxel within which to measure the required quantity. The average values of each voxel are then arranged in a matrix in an ASCII file which can be processed later.

There are various programs that can be used in parallel with FLUKA, one of them is Flair (FLUKA Advance Interface). This program acts as a graphic interface of FLUKA, through which it is possible to manage all the aspects listed above without having to directly modify the ASCII input file. There are 5 sections located at the top of the program: “Flair”, “Input”, “Geometry”, “Run” and “Plot”.

Through the Flair section it is possible to generate a new file. The source, geometry, materials, physical parameters, simulation parameters and scoring will be described in the “Input” section. In this it is possible to add and remove CARDs according to the need of the simulation. The Flair program automatically generates the ASCII file with the '.inp' extension while compiling the “Input” section.

The Flair program is also equipped with a Geometry-Editor that allows to work on 2D sections of the geometry. The visualization is interactive, in fact the preprocessing of the data ensures that errors are reported graphically. It can be accessed through the "Geometry" section. Finally, through the "Run" section it is possible to start the simulation and observe its status and through the "Plot" section it is possible to plot the results obtained from scoring.

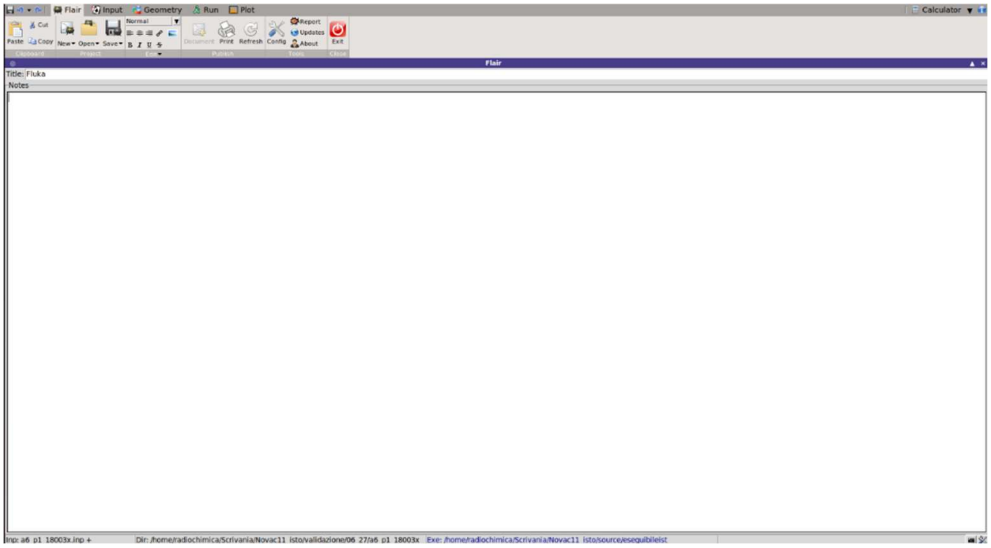

Figure 2.4 Flair open-window

Gamma Test

Determining the level of agreement of two dose profiles can be complex. This is because dose profiles, particularly those of electrons, very often have both low gradient regions (plateu) and high gradient regions. The simplest method of evaluating the agreement between two profiles is the point-by-point comparison, in which the difference in dose at each point of the profile is evaluated. The method provides robust results in low gradient regions, on the contrary in high gradient regions it tends to over-emphasize any difference in dose. Take for example the image shown:

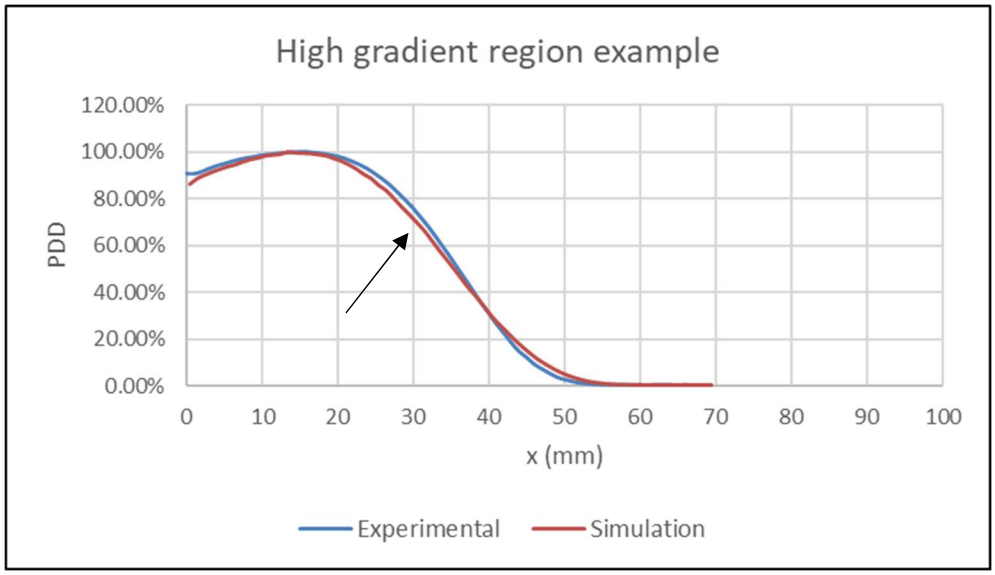

Figure 2.5 High gradient region example

At depth $x_0 = 30mm$ the difference in percentage dose between the two distributions is considerable, but if the difference in dose at x_0 and x_0+dx_0 is compared, where dx_0 is a fraction of millimeters, it is practically in agreement.

More complex comparison methods were therefore introduced that also take into account the contribution of high gradient areas. One of the most used is the Gamma Test [48, 49]. This method is based on the measurement of a gamma value for each point of the reference profile with respect to all points of the compared profile. The calculation of the gamma value is repeated for each point of the reference profile and for each of these points the minimum value

returned by the Gamma function as a result of the test is chosen. If this parameter is less than 1, the point studied is in accordance with the chosen parameters, otherwise it is not. The Gamma function is evaluated as follows:

$$\gamma = \sqrt{\frac{(r_i - r_0)^2}{\Delta r^2} + \frac{(D_i - D_0)^2}{\Delta D^2}} \tag{2.10}$$

Where:

- γ is the result of the test ($\gamma > 1$ the points are not in agreement, $\gamma < 1$ the points are in agreement).
- r_i is the geometric coordinate of the profile to be compared.
- r_0 is the geometric coordinate of the reference profile.
- D_i is the dose of the profile to be compared evaluated in r_i.
- D_0 is the dose of the reference profile evaluated in r_0.
- ΔD is the "dose-difference" parameter.
- Δr is the"distance-to-agreement" parameter (DTA).

The two parameters, ΔD and Δr, are chosen arbitrarily and respectively indicate the maximum value of difference in dose and spatial displacement that can be present between two points so that they are considered to be in agreement. As these increase, the test becomes more permissive, on the contrary, as these decrease it becomes more restrictive.
The classic parameters used in EBRT radiotherapy are 3% / 3mm [48, 49], but in this work they are set at 2% / 2mm.
It is important to emphasize that the "dose-difference" parameter is defined with respect to the maximum dose of the entire profile.
From a geometric point of view, the result of the gamma test returns the radius, normalized through the parameters ΔD and Δr of a circle centered in (r_0, D_0) and intersecting the point (r_i, D_i). That is, it is the minimum distance between the two points (r_0, D_0) and (r_i, D_i). These last geometric considerations are valid if the geometric coordinate is expressed in a single dimension r and therefore the system consists of two total dimensions (r, D). The test has value even if the number of geometric dimensions is increased and the interpretation of

the result value is always the same: "the multidimensional distance between the measurement and calculation points in both the dose and the physical distance, scaled as a fraction of the acceptance criteria "[49].

It has already been specified that two points from two dose distributions are in agreement if they have a gamma test result lower than 1. Overall two distributions are said to be in agreement if 95% of the points presents γ <1.

In order to perform the Gamma test, a Matlab algorithm was written to compare the reference profiles, obtained experimentally, with those to be compared, resulting from the FLUKA simulations. To increase the robustness of the test, it was decided to perform a linear interpolation of the profile obtained through simulations in order to have a greater number of points to compare. This is necessary since the spatial sampling of FLUKA data is very similar to the selected Δr (1 mm vs 2 mm). If no interpolation was performed, significant underestimation of γ are possible in high gradient region.

The Matlab code is the following:

```
%define vectors
simulation_vector = xlsread("Simulazione_interpolato.xlsx");
experimental_vector = xlsread('Sperimentale.xlsx');
x = linspace (0,69,70);
x = x';
x_new = linspace (0,69,70000);
x_new = x_new';
D = interp1(x,simulation_vector,x_new,"linear");
D0 = experimental_vector;

%define gamma test parameters
dose_parameter = 0.02;
d = dose_parameter;
space_parameter = 2;
r = space_parameter;

%vectors lengh
z = numel(D);
y = numel(D0);

s0 = x;
s = x_new;

%gamma test
for j = 1:y
    for i = 1:z
       gamma_test (i) = ((((D(i,1)-D0(j,1))^2)/d^2)+((s(i)-s0(j))^2)/r^2)^(1/2);
    end
    result (j) = min(gamma_test);
end

result_good = numel(find(result<1));
test = (result_good+1) / y
% +1 because first experimental value has not a physical meaning
if test >= 0.95
    disp('job done')
    else
    disp('fail')
end

errori = find (result>1);
```

Figure 2.6 Screenshot of the Matlab algorithm to evaluate the Gamma Test

Chapter 3

Introduction to the validation process

In this chapter the process followed for the validation of the Monte Carlo code is illustrated. As previously specified, validation involves the implementation of the simulation parameters in order to obtain a result equal to the experimental result within a certain error. First of all it was decided to compare, as a result, the PDD (the percentage depth dose curve) of the experimental measurement with that of the simulation evaluated along the clinical axis of the beam. The choice of using the PDD, i.e. the dose profile normalized to its maximum value, has two reasons. First it is a measure independent of the dose quantity. Secondly, the experimental measurement is obtained as a dose response of a microdiamond detector. On the contrary, Fluka, as will be illustrated later, returns the average dose in the studied point given by a single primary electron. These two quantities are therefore not comparable thus.

Initially the validation process was focused on the simulation performed with the circular applicator with a diameter of 10 cm and a 80 cm SSD at a nominal energy of 10 MeV. This is in fact the reference geometry for what concerns the applicators. Subsequently, the circular applicators with diameters of 6 and 5 cm, each of these 65 cm long, were validated at a nominal energy of 10 MeV. The validation of the latter also involved the comparison of the simulated and experimental Output Factors (OF). OF is defined as the ratio between the dose of any applicator and the dose of the reference applicator at the build-up points of the respective curves.

As already illustrated, the comparison of two curves in radiotherapy can be complex due to the presence of high gradient regions. Reason why a simple point-by-point evaluation is not enough. The Gamma Test was therefore used, setting the dose and DTA parameters respectively to 2% / 2mm.

The experimental measurements are provided by ASST Papa Giovanni XXIII (Bergamo) and are those characteristics of the Novac-11 accelerator and the various applicators used in this hospital. In fact, the applicators are "personal" and can be modified ad personam.
The experimental set-up involves a 30 cm deep rectangular phantom filled with water in which a motorized system is installed inside that allows the movement of the micro-diamond detector. The measurement of the microdiamond is subject to a maximum uncertainty of 1%.
The Fluka script, which will be illustrated in the next paragraph, was written starting from technical drawings provided by the manufacturer of the LINAC.

FLUKA script

In the previous chapter, the basic steps involved in the development of a simulation were illustrated, the main parts of the Input (Primary, Physics, Geometry, Score) and the Run that make up the FLUKA script are presented below.

Primary

The "Primary" section describes the characteristics of the source and its position in space.

Figure 3.1 CARDs for the description of the source in the FLUKA script

The "BEAM" CARD allows the selection of the primary particle to be transported, "ELECTRON" in this case, its energy and eventually the spatial characteristics of the beam.
The point where the source is located is instead described with the "BEAMPOS" CARD, in this case (0; 0; -0.1).
The "BEAM" CARD in this work has been overwritten by an external input file written in FORTRAN 77, FLUKA native programming language. In fact, FLUKA allows to modify the

CARDs with user defined .inp scripts to describe characteristics of some aspects of the problem not taken into consideration by the precompiled CARDs. In particular, the default "BEAM" CARD provides a description of the energy spectrum only via monoenergetic or symmetrical (Gaussian or rectangular) distributions. The IORT treatment provides for a diffuse dose contribution of up to 40%, which is why it was necessary to describe an asymmetric spectrum that also had a low-energy component.

The description of the spectrum took place through a discrete histograms spectrum, which was constructed through the approximation of a skew normal distribution. This is a continuous probability distribution that generalizes the normal distribution to allow for non-zero skewness. It is described by an average energy μ, a standard deviation σ and an asymmetry coefficient α.

The .inp script that describes the histograms and sampling from them is quite simple. For the sampling of the histograms the rejection sampling method was used, exploiting a uniform distribution.

The written code is briefly illustrated:

```
RVX = FLRNDM(UGH)*RVINT+RVMIN
RVY = HMAX*FLRNDM(UGH)

IF (RVX .GE. RVMIN .AND. RVX .LT. (RVMIN + DELTA)) THEN
   IF (RVY .LE. H1) THEN
      PM0FLK = ((RVMIN + (RVMIN + DELTA)) / 2) / 1.D3
   END IF
END IF
```

Figure 3.2 Initial part of the FORTRAN 77 code that describes the source in the user .inp script

FLRNDM (UGH) is the FLUKA command that allows to generate a random number in the interval [0,1). RVX and RVY are respectively any number within the histogram domain and any number in the interval [0, maximum histogram height). The code will then consist of the repetition of a series of double IF cycles, one for each bin of the histogram, which describe the sampling through rejection sampling. The first IF attributes RVX to the bar of the histogram in which it falls, the second IF instead decides whether to accept or reject the value. If the value is accepted, PM0FLK is equal to the average value of the extremes of the histogram bar in

which the value fell. PM0FLK is the variable that describes the energy of the particle in the FLUKA script. PM0FLK is then divided by 1000 since the energy in FLUKA is described in GeV while the histogram in MeV.

The procedure will be repeated for each simulated primary. With a sufficiently large number of simulated primaries, the energy distribution of the simulated electrons will be very similar to that described by the histogram.

Physics

The "Physics" section describes the type of interactions to be simulated and the approximations adopted. The transport of electrons in matter in FLUKA is in fact simulated through a "condensed history method", in which the cumulative effects of multiple electron collisions are approximated in a single "step".

Figure 3.3 CARDs for the description of the physical approximation adopted in the FLUKA script

The "EMF" CARD enables the transport of electrons, positrons and photons. The following phenomena will then be simulated:

- Rayleigh scattering and Compton scattering
- Photoelectric effect
- Bremstrahlung's X-rays production

With the CARD "MULSOPT" the tracking conditions for multiple Coulomb scattering are imposed. A maximum of 5 single scattering events at region boundary crossing were simulated only for electrons and positrons, the latter aspect is chosen through the "GLOBEMF" WHAT.

The "EMCUT" CARD sets the energy thresholds for electron and photon transport cutoffs in selected regions. It also allows to set an arbitrary energy threshold for all electron and photon

interactions managed by EMF on a material basis. This is of course non-physical, but serves to improve the computational performance of the code, since simulation of interactions at very small energy can be quite time consuming without having a relevant effect on the overall accuracy of the simulation at the macroscopic scale. It is used to describe the transport in the region P22, that corresponds to the simulated water phatom. Transport cutoff energies were set to 100 keV and 10 keV for electrons/positrons and photons, respectively.

On the contrary the "EMFFIX" CARD sets the size of electron steps corresponding to a fixed fraction of the total energy. The setting is done by material, giving as many "EMFFIX" definitions as needed. Maximum single step energy loss for electrons was set to 1% of the total energy in the phantom and 3% of total energy in all other materials.

At last the "STEPSIZE" CARD sets the minimum and maximum step size on a region-by-region basis for transport of all charged particles. The step size is set between 0,01 cm and 0,1 cm.

Geometry

The principles of the construction of the geometry of the simulated set up have already been illustrated in the previous chapter. The section of the FLUKA code relating to the description of the geometry is introduced by the "GEOBEGIN" CARD and closed by the "GEOEND" CARD.

Through the "ASSIGMA" CARD a material can be assigned to each described region. The material will be previously described through the "MATERIAL" CARD. This can be used individually to describe a single-element material or coupled to the "COMPOUND" CARD to describe an alloy or a compound.

The geometry of the set up features a parallelepiped-shaped phantom, the applicator, body and head of the accelerator, the titanium filter and two sets of parallel plate ionization chambers which are used to monitor the output of the accelerator.

The source is positioned just before the titanium filter (in *Figure 3.4* this is identified by the conjunction of the two dashed axes).

The "water" material is attributed to the target phantom, the "PMMA" material to the applicator and finally the "titanium" material to the titanium filter. It must be considered that the detailed description of the setup is dictated by the knowledge of the accelerator as provided by the manufacturer. In fact, it is not known if there are other filters placed between the exit of the accelerator cavity and the titanium filter. This latter concept will be better explained later in the paragraph "source".

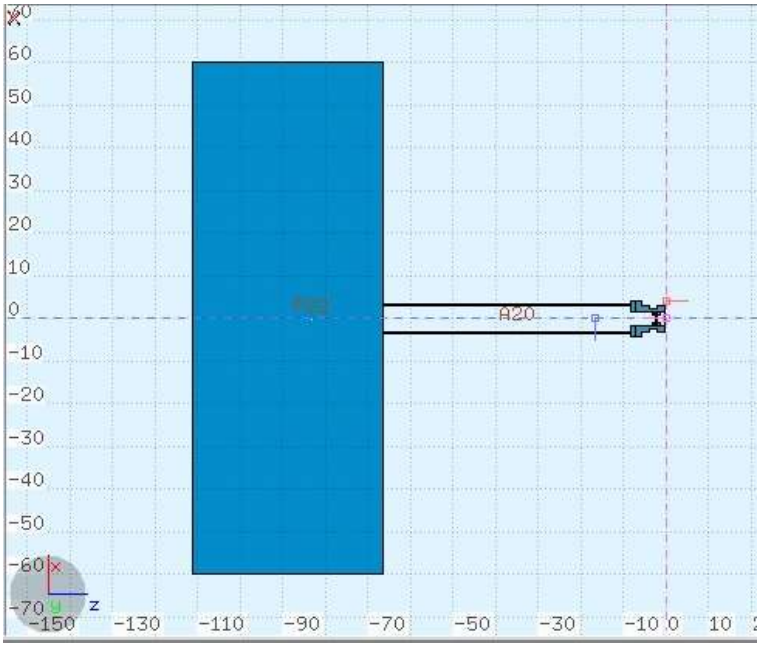

Figure 3.4 Representation of the experimental setup's geometry made by Flair

Score

In the "Score" section the fictitious detectors that report the desired output are defined.

Figure 3.5 CARDs for the description of the simulation's score in the FLUKA script

In the validation process the "USRBIN" CARD and the "USRBDX" CARD were employed. The first one scores distributions of several quantities in a regular spatial structure (binning

detector) independent from the geometry. Both “USRBIN” CARDs return the dose quantity according to two different geometric meshes. The first one presents a cubic mesh of 1 mm^3 voxels. The second one is a cylindrical mesh defined on the surface of the phantom with spatial bins of 1 mm and 2.5 mm along depth and radial direction, respectively. The dose at a point is calculated as the average of the dose released by each primary electron in the voxel. A “dose per electron per voxel” value is indeed returned.

On the contrary, the "USRBDX" CARDs give us back the energy spectrum of the electrons and photons that reach the surface of the water phantom. These CARDs return the number of the selected particle generated from the single primary particle’s interactions distributed according to the energy spectrum.

The Scores obtained through the CARDs are then reprocessed through MATLAB codes.

Run

The simulations useful for the validation process were performed with 350 million primaries. This condition makes it possible to obtain a relative error of the scored dose values of less than 1% for each point of the clinical axis at least up to a depth of R20. This value was chosen because it is the point where the penumbra zone ends. In the field of radiotherapy, penumbra is defined precisely as the region that undergoes a dose amount between 80% and 20% of the maximum dose.

Source

The validation process focused on the description of the energy spectrum of the source of the primary electrons. In fact, once the physical and geometric simulation parameters that best described the real case were set, it has been necessary to modify the energy spectrum of the electrons in order to obtain a good correlation between the experimental PDD and that obtained through the simulation. It must be emphasized that the simulated irradiations have a nominal energy of 10 MeV, which does not correspond to the fact that the accelerator emits

a monoenergetic beam at 10 MeV [50, 51]. The source is defined as a point source with Gaussian spatial distribution (0.5 mm FWHM) along the x and y transverse directions, the z-axis being coincident with beam axis.

As already mentioned in the introductory chapter, the PDD obtained by irradiating a phantom with an IORT accelerator is characterized by a greater dose contribution on the surface, a shallower R_{100} and a decrease in the amount of dose in depth compared to the PDD obtained by irradiation with a EBRT accelerator at the same nominal energy. In fact, the IORT applicator generates a diffuse dose contribution that reaches up to 40%. This component of low-energy electrons and Bremsstrahlung's X-rays considerably increases the surface dose component [1]. Furthermore, it should be considered that the region around the R100 for the PDD of an IORT treatment presents a more gentle trend, almost a plateau. Both in the case of the experimental measurement and the computational result, the value of R_{100} is included in a range of a few millimeters. In fact, the uncertainties are respectively 1% for the microdiamond detector and 0.3% for the FLUKA simulation (performed with 350 million primaries) around R_{100}, sufficient to result in significant uncertainties on the exact position of the profile maximum. As an example, the experimental measurement of the 6 cm circular applicator is taken: the maximum dose is measured in two distinct adjacent points, the R100 is indeed identified both at a depth of 15 mm and at 16 mm.

The validation process began by finding the energy of a monoenergetic beam that would return the best approximation of the R50. The use of symmetric, Gaussian and rectangular energy distributions was then investigated. Especially the first gave excellent approximations either in the surface component of the curve or in the deep one as the standard deviation varied, but never in both with the same standard deviation. It was therefore decided, also with respect to the considerations on the spectra explained above, to implement an asymmetrical distribution with a low energy component.

As mentioned at the beginning of the chapter, the construction of the histograms was done starting from a skew normal distribution. In particular, each histogram, 1 MeV wide, will have a height equal to the average of the skew normal distribution in that energy range.

The skew normal distribution that yielded the best correlation was found to be described by a mean of 12, a standard deviation of 3.5, and an asymmetry factor of -100. The distribution is shown below in *Figure 3.6*.

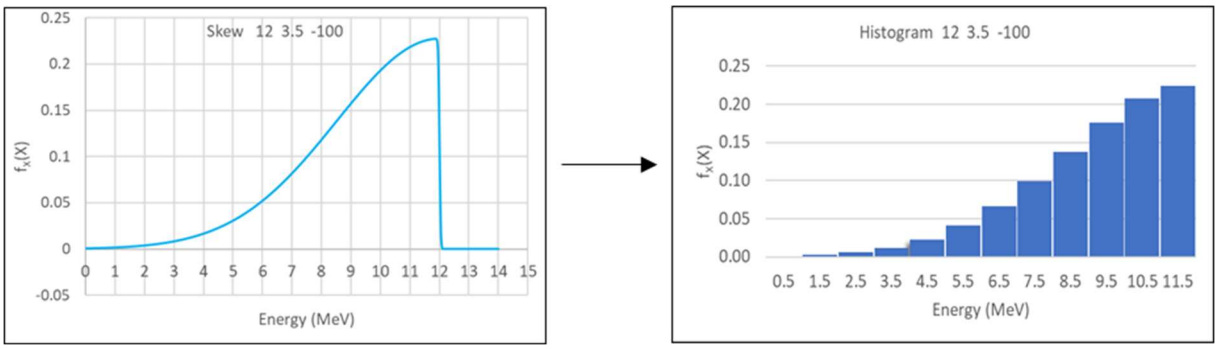

Figure 3.6 The skew normal distribution with parameters μ = 12, σ = 3.5 e α = -100 and the histogram obtained from that

Finally, the last histogram was slightly lowered to obtain an even better approximation

The presence of an important contribution to low energy could also be justified by the presence of additional filters between the titanium filter and the accelerator injector not described in the drawings provided by the manufacturer for reasons of trade secret.

Nonetheless, the energy spectrum found is in agreement with those found in previous literature works [51, 52]. The first work in particular is performed on a Novac-7, an older version of the Novac-11, which shares the same hardware. In addition, there does not seem to be any work currently being done on the Novac-11 in the literature.

The only difference that can be pointed out is that the low-energy region has a steeper descent for the previous works. This last observation supports the suspicion that there may be an additional filter not specified by the manufacturer.

Validation result

The validation results for the applicators studied are reported in the following as a comparison between simulated and experimental values.

The experimental PDD measurement is obtained through 70 measurements, one every millimeter, along the clinical axis of the beam (0; 0; Z).

The computational measurement is instead obtained through the "USRBIN" CARD with a cubic mesh of 1 mm^3 volume by extracting the first 70 dose values along the clinical axis of the beam (0; 0; Z).

Circular applicator with a diameter of 10 cm, SSD (skin-source distance) 100 cm, nominal energy 10 MeV, PDD evaluated along the clinical axis of the beam (0; 0; Z)

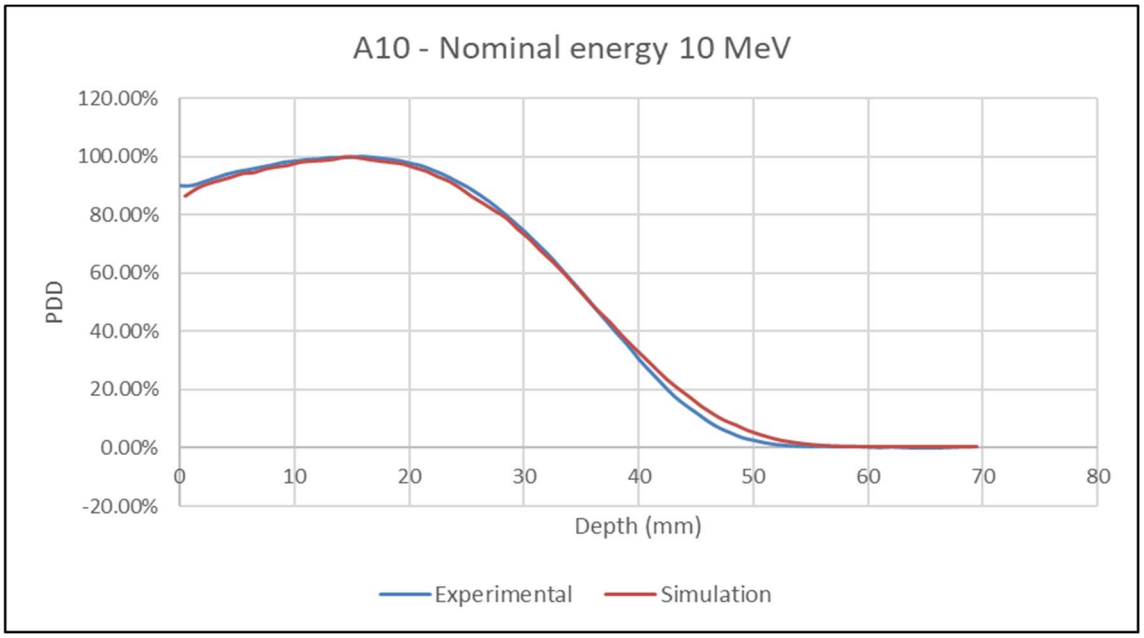

Figure 3.7 Comparison between the experimental PDD and that obtained through FLUKA simulation for the 10 cm circular applicator at a nominal energy 10 MeV

Circular applicator with a diameter of 6 cm, SSD (skin-source distance) 65 cm, nominal energy 10 MeV, PDD evaluated along the clinical axis of the beam (0; 0; Z)

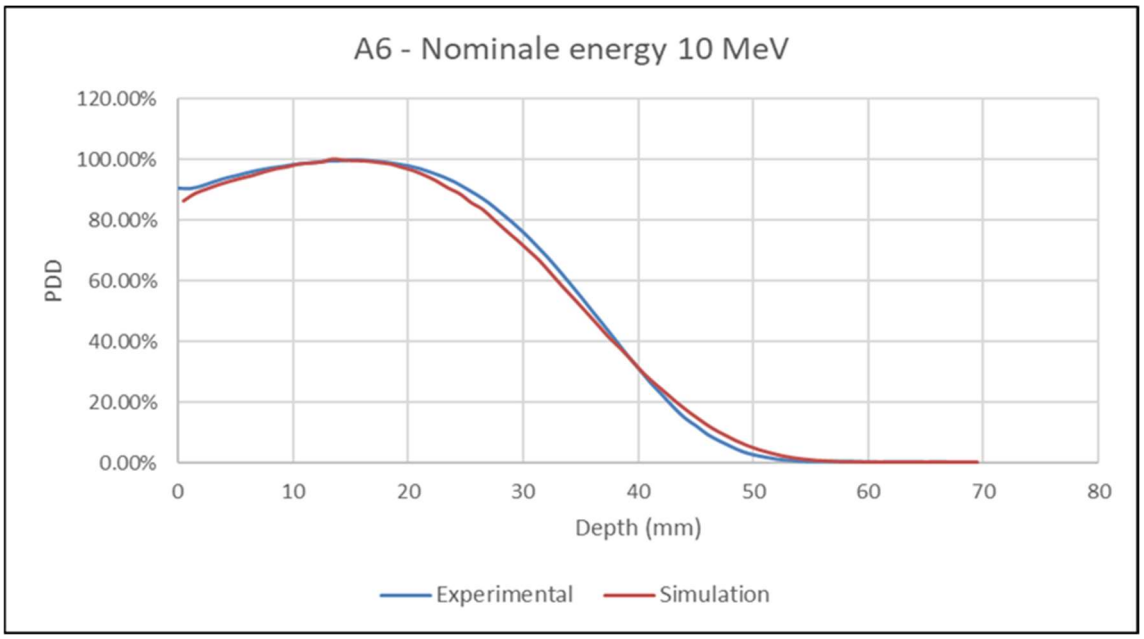

Figure 3.8 Comparison between the experimental PDD and that obtained through FLUKA simulation for the 6 cm circular applicator at a nominal energy 10 MeV

Circular applicator with a diameter of 5 cm, SSD (skin-source distance) 65 cm, nominal energy 10 MeV, PDD evaluated along the clinical axis of the beam (0; 0; Z)

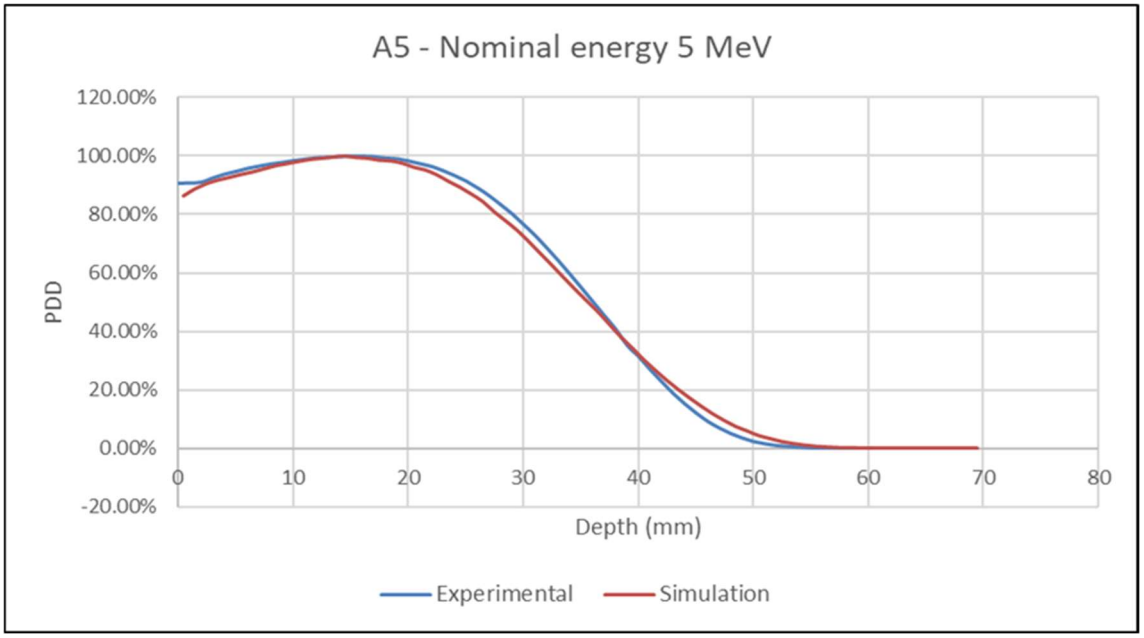

Figure 3.9 Comparison between the experimental PDD and that obtained through FLUKA simulation for the 5 cm circular applicator at a nominal energy 10 MeV

Summary of main numerical validation results

10 CM APPLICATOR	Simulated	Measured
Gamma Test 2mm/2%	100%	
Gamma Test 1mm/1%	85%	
R100	14.5 mm	16 mm
R90	24 mm	24.5 mm
R50	36 mm	35.5 mm
R30	41 mm	40.5 mm
6 CM APPLICATOR		
Gamma Test 2mm/2%	100%	
Gamma Test 1mm/1%	60%	
R100	15 mm	13.5 mm
R90	25.5 mm	24 mm
R50	35.5 mm	35 mm
R30	40.5 mm	40 mm
OF	96%	
5 CM APPLICATOR		
Gamma Test 2mm/2%	100%	
Gamma Test 1mm/1%	63%	
R100	15 mm-16 mm	14.5 mm
R90	25.5 mm	24 mm
R50	36.5 mm	36 mm
R30	40.5 mm	41 mm
OF	95%	

Table 1 Main numerical validation results

Energy spectrum

Lastly, it was decided to analyze the energy spectra of the electrons and photons that reach the surface of the water phantom. These are not validated by any experimental measure, but they provide a reasonable result and their trend is in agreement with those evalueted for Novac-7 [1] and reported in *Figure 1.4*.
As previously described, FLUKA returns the average value of particles (photons or electrons) that reach the surface per primary, this quantity is reported on the Y axes.

Energy spectrum of electrons at the surface of the water phantom

The spectrum of the electrons at the surface of the water phantom obtained is very similar to that described in the source. However it also presents a certain degradation component of the beam due to the interation between electrons and the applicator and air. Having described the source as the sum of monergetic beams, the spectrum at the surface of the water phantom, as can be seen from *Figure 3.10*, appears as a sum of peaks, centered in the energy of the various monoergetic sources. Having chosen this description for the source, the degradation component is well observable between one peak and another. The energy spectrum of the 6 cm circular applicator is shown as an example. The spectra of the other two applicators are not reported as they are very similar.

Energy spectrum of photons at the surface of the water phantom

Providing an important component of bremsstrahlung X-rays due to the interation between electrons and the applicator, it was decided to study the spectrum of photons at the surface of the water phantom as well.
The energy spectra obteined have a low energy peak, between 50 and 100 keV for all three applicators, and then have a fairly fast decreasing trend. The result, which is not validated by any experimental measure as already said, returns a more than reasonable trend. The 10 cm circular applicator has a much more important component of photon production.

This in fact is 20 cm longer than the other two thus increasing the probability of interactions between electrons and applicator and so the possible generation of X-rays.

It also seems that as the applicator diameter decreases, the number of photons generated decreases.

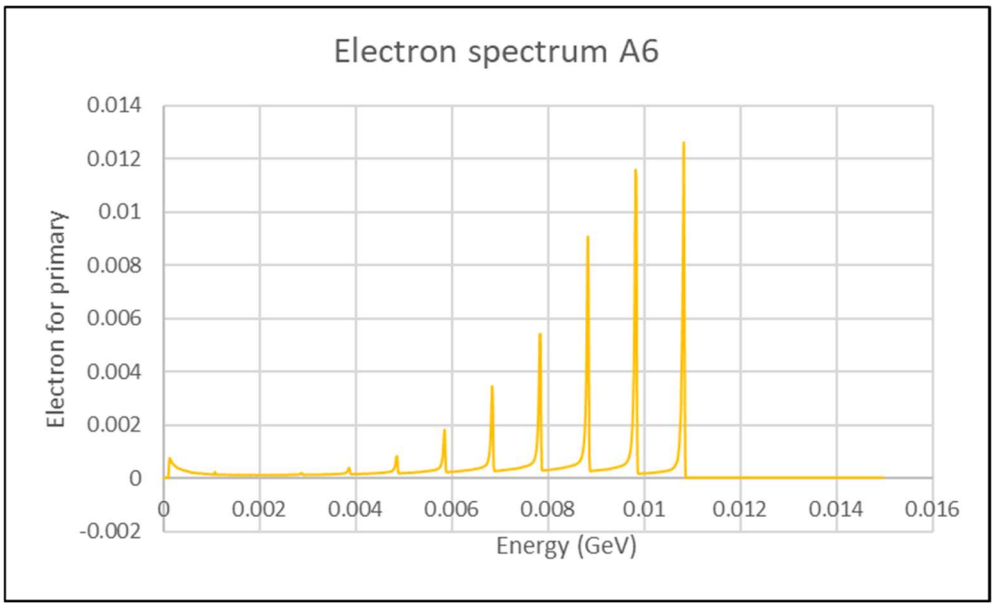

Figure 3.10 Energy spectrum of electrons at the phantom surface for the 6 cm circular applicator

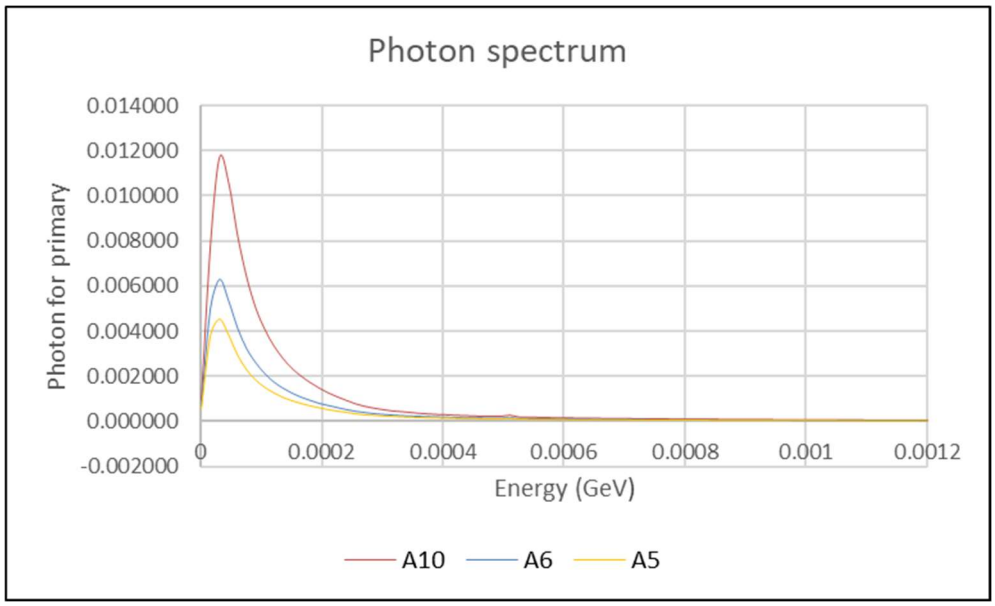

Figure3.11 Photon spectra of the three different applicators at the phantom surface

Chapter 4

Clinical conditions

In the introductory chapter, the advantages of IORT treatment compared to traditional EBRT were described, deriving from the fact that the treatment is delivered directly in the operating room through mobile linear accelerators. It was also emphasized that, by providing the treatment directly in the operating room, there is the possibility of using radiation shielding disks, which are surgically implanted in the region posterior to the target, and other devices.
In this chapter we want to focus on the beneficial effects offered by the devices that can be used during treatment. These are precisely radiation shielding disks, applicator bolus and possibly a radioprotection vest. The focus was on those in use at the ASST Papa Giovanni XXIII hospital (Bergamo).
The previous chapter described the validation process of the Monte Carlo code which made it possible to identify the reference conditions for each applicator.
In this chapter the variations of the system response to the introduction of the various devices used will be presented, highlighting any advantages and disadvantages of their use.
In this chapter, the reference conditions do not refer to those indicated by international guidelines, ie the use of the 100mm applicator, but refers to the response of the system without the use of any device for any applicator.
The radiation shielding disks have the task of limiting the dose to the tissues posterior to the target. These were initially made of water equivalent plastic material, generally PMMA, which do not substantially modify the PDD but simply absorb the dose of the patient's tissues they displace [54]. On the contrary, the use of a disk of high-Z material imposes a greater shielding factor of the posterior tissues [8, 9, 10, 54]. However this kind of disks generates an important backscattering component that must be shielded with an additional low-Z layer placed between the target and the high Z disk [8, 9, 10, 54]. The manufacturer of Novac-11 (Sordina

S.p.A.) suggests the use of a 3 mm thick steel (AISI 316L) disk coupled with a 5 mm thick polyether-ether-ketone (PEEK plastic) disk. At the ASST Papa Giovanni XXIII hospital (Bergamo), a pair of lead and aluminum disks, both with a thickness of 5 mm, are also used as an alternative. Regardless of the material they are made of, the disks always have a circular geometry with a diameter of 2 cm larger than that of the applicator. The composition of the disk materials considered for simulation is shown in Appendix A.

The usefulness of the applicator bolus has already been extensively described in Chapter 1. This is used to avoid tissue herniation in the applicator, to uniform the irradiation field and possibly to allow the first millimeters of the target to receive an isodose of 90%. The bolus has a cylindrical geometry, with a diameter of two centimeters greater than the applicator and a height of a few millimeters. It is made of PMMA, a water-equivalent plastic material.

The radiation protection vest is instead used to avoid dose to the skin surrounding the applicator. In fact, it is expected that there is a component of leakage electrons from the applicator and also a component of Bremsstrahlung X-rays generated inside the applicator. Since the skin is a particularly radiosensitive organ, it was seen that it was necessary to first investigate the total amount of dose received in reference conditions and secondly the possible beneficial effect of using an ad hoc radiation protection vest for the patient. It was decided to simulate the use of a radiation protection vest consisting of a 0.5 mm layer of lead and one consisting of a 1 cm layer of water equivalent material.

In clinical practice, the nominal dose prescribed in the treatment plan to be delivered to the patient does not account for the presence of the devices or any positive or negative effects of these. This is equivalent to assuming that there is no perturbation in terms of dose. This chapter intends to verify whether the latter assumption is acceptable or not.

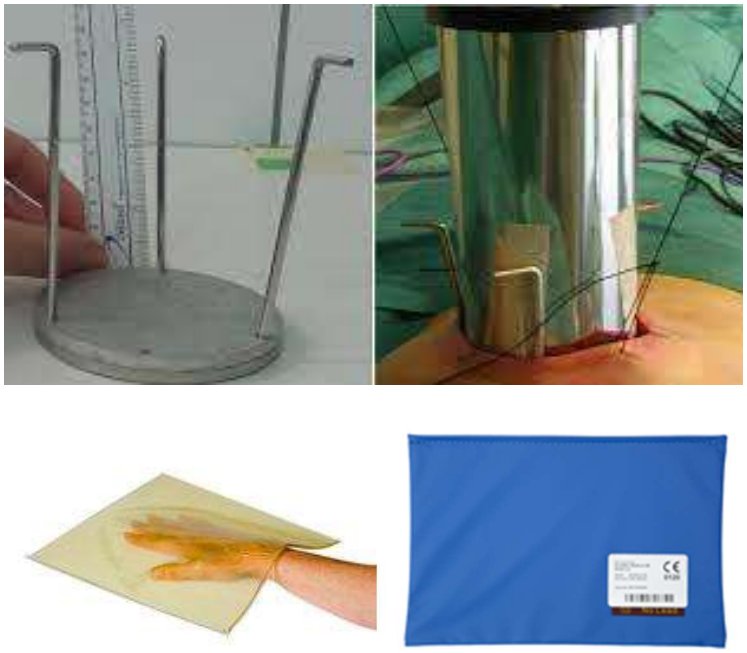

Figure 4.1 A disk, a bolus and a radiation protection vest used during a IORT treatment (Infab Co. and MEDTEC, Inc.).

Radiation shielding disks

In radiotherapy it is customary to indicate with PTV (Planning Target Volume) the volume upon which the planning of the treatment is effectively performed and which will have to receive the prescribed dose. In addition to the gross tumor volume (GTV), the PTV also considers the effect of all possible geometric variations and uncertainties in order to ensure that the prescribed dose is effectively absorbed in the clinical target volume (CTV). The latter indicates the volume in which the gross tumor is included and the surrounding region in which there is the possibility of finding other metastatic cells.

In the context of IORT treatment these definitions are not taken into consideration. As already described in the first chapter, IORT is mainly used to sterilize the tumor bed after it is removed, such that a GTV is not actually identifiable. The volume to be treated is generally called target. The radiation shielding disks are therefore placed just after the end of the target. By placing one of these devices at depth X, a target between the skin and depth X is automatically defined.

The radiation shielding disk is always placed perpendicular to the clinical axis of the beam in order to obtain uniform irradiation throughout the volume of the target. In fact, in the literature there are various works that show how a non-perfect positioning of the disk then imposes a non-uniform dose to the whole volume [55].

The analysis on the variation of the dose profile due to the presence of a radiation shielding disk is performed only in one dimension, along the clinical axis of the beam (0, 0, Z). In the region between the skin and the disk, a certain increase in dose is expected due to the phenomenon of backscattering. In the posterior region of the disk, on the other hand, a significant decrease in the amount of dose is expected due to its shielding capacity.

As already highlighted, two pairs of disks will be simulated: one in aluminum-lead (both 5mm thick) and one in PEEK-steel (5mm and 3mm thick respectively). The simulations will cover target sizes: 10mm, 15mm, 20mm, 25mm and 30mm.

Any differences between the two types of radiation shielding disks between use at various depths will be highlighted.

In order to provide a description as complete as possible, the following parameters were used to describe the effect induced by the radiation shielding disks: PDD, Backscatteing Factor (BF), Transmission Factor (TF), Dose Difference (DD), Clinic Variation (CV). These are described in the next paragraphs.

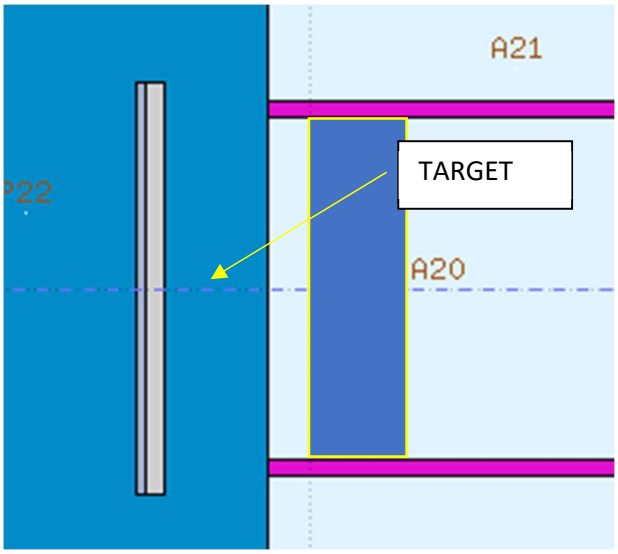

Figure 4.2 FLUKA implementation of geometry with radiation shielding disk

PDD (Percentage Depth Dose) definition

Percentage dose profile observed in the presence of the radiation shielding disk normalized for the maximum dose value in reference conditions. The dose in the region where the disk is present is set to 0.

The profile is normalized for the maximum dose value in reference conditions, i.e. in absence of the disk, in order to observe any areas in which the isodose exceeds 105%, leaving the prescribed dose region, and being able to directly perform a comparison between the PDD in reference conditions and the one in the presence of the disk.

$$PDD(z) = \frac{D_{disk,i}(z)}{D_{rif}(z_{max})}\% \tag{4.1}$$

Backscattering Factor (BF) definition

The Backscattering Factor describes the percentage change in dose between the condition in the presence of the disk and the reference condition at each depth z.

$$BF(z) = \frac{D_{disk,i}(z)}{D_{rif,i}(z)}\% \tag{4.2}$$

This is calculated for all points of the target. Having described with FLUKA a mesh with a level of discretion of 1 mm, for a target of *X* mm *X* Backscattering Factors will be expected.

Transmission Factor (TF) definition

The Transmission Factor describes the percentage change in dose between the condition in the presence of the disk and the reference condition.

$$TF = \frac{D_{disk}}{D_{rif}}\% \tag{4.3}$$

This is calculated in the first point downstream the radiation shielding disks.

Dose Difference (DD) definition

The Dose Difference is calculated as the sum of the differences between the two dose profiles normalized for the maximum dose value of the reference profile, divided by the number of points at which the assessments are made.

$$DD = \frac{\sum_i^n \frac{(D_{disk,i} - D_{rif,i})}{D_{rif,max}}}{n} \tag{4.4}$$

The summation is divided by the number of points so that two Dose Difference targets with different sizes can be compared.

This parameter underlines if there is an increase or a decrease of the dose along the clinical axis.

Clinical Variation (CV) definition

The Clinical Variation aims to observe the differences in the values included in the 90% -105% isodose range in the case of the reference condition and in the presence of the disk along the clinical axis of the beam (0; 0; Z).

A linear interpolation of the PDD values is performed for both the disk profile and the reference profile to improve the statistics, in a range between the phantom surface and the disk

depth, and the quantity of points outside the 90% -105% range is evaluated. Indicating with Y the points that fall within the range:

$$CV = Y_{disk} - Y_{rif} \quad (4.5)$$

A positive CV value indicates a therapeutic advantage given by the presence of the disk, a negative value on the contrary a therapeutic disadvantage. That is, the target having to receive a value between 90% and 105% of the nominal dose, any backscattering effects could increase the region that meets this criterion or decrease it. 105% is taken as the maximum acceptable level of overdose

Dosimetric effect of radiation shielding disks

The simulations in the presence of the radiation shielding disks are performed with 150 million total primaries, sufficient to have an error of less than 1% in the target area and for each parameter described above. At the end of the two paragraphs "Al-Pb disk" and "PEEK-steel disk" there are summarizing graphs of the most significant numerical data. In particular, the PDDs for all applicators are shown. While for the Backscattering Factor and the Transmission Factor, only the trends for the 5 cm and 6 cm applicators are reported respectively, since, as will be explained later, the trends are similar for all three applicators. The numerical values are instead tabulated in Appendix B.

Al-Pb disk

The aluminum-lead radiation shielding disk has an excellent radiation shielding capacity. For each applicator and for each target, a transmission factor lower than 1% is observed. Especially for superficial targets this allows to save considerable dose to the patient. PDD values at the depth where TF is measured vary from approximately 0.8% for superficial targets to 0.3% for deep targets.

In the case of a 1 cm target, for example, for each applicator in reference conditions, PDD is worth about 98% at a depth of 10.5 mm, i.e. where the disk would start for a 1 cm target. On

the contrary, in the presence of an aluminum-lead disk, considering a TF of about 0.8% for each applicator, the PDD is worth about 0.8%. An IORT treatment provides for the delivery of about 20 Gy in a single session, so that healthy tissue at a depth of 10.5 mm receives about 19 Gy less in the presence of this kind of disk.

The Backscattering Factor instead presents values of about 108% -110% in the first point before the disk, the values decrease as the depth decreases. The effect of the backscattering phenomenon is well observable in the first mm before the disk, after which the BF assumes values between 100% and 101% in the following millimeters such that it becomes almost negligible, also considering that the value of the statistical uncertainty is of about 0.5%. For each applicator and for each target the BF has a similar trend. *Figure 4.10* is shown as an example, which shows the BF trend for the 6 cm applicator. The values seem to decrease faster for deeper targets.

For the more superficial targets (1 cm, 1.5 cm, 2 cm) the backscattering phenomenon imposes a PDD over 105% for some points before the disk. The phenomenon is more observable for the 1.5 cm target since the build up for a beam with a nominal energy of 10 MeV is placed at around 15 mm depth. It follows that the 1.5 cm target is the most sensitive to the backscattering phenomenon.

These last observations are also confirmed by the study of the Clinical Variation parameter. This assumes a negative value, i.e. there are fewer points of the PDD between 90% and 105% compared to the reference condition, for the 1 cm, 1.5 cm and 2 cm targets for each applicator. In particular, the 1.5 cm target always has the worst CV with a value around -10%. It must be considered that the CV value also depends on the statistical variations of the simulations, which, not being performed with the same seed, do not give the same result in statistical terms. It follows that CV values equal to a few percentage points cannot be taken as totally reliable due to related uncertainty. The backscattering phenomenon almost never has a positive effect from a clinical point of view. In fact, the 1 cm, 1.5 cm and 2 cm targets show PDDs, in the target region, well above 90% already in reference conditions. The 3 cm target, on the other hand, has a PDD value in the millimeters before the disk well below 90% in the reference condition, such that the backscattering phenomenon is not sufficient to reach that

level. Only the 2.5 cm target seems to have some positive effect. In fact, in reference conditions for all three applicators, R90 is set at about 25 mm, exactly the size of the target, so that by positioning the disc it is ensured that all the target is irradiated in the correct isodose range.
Finally, the Dose Difference value has similar values for all three applicators. The 1 cm target shows an increase of approximately + 3%, the 1.5 cm target of approximately + 2%, the 2 cm target of approximately + 1.5%, the 2.5 cm target of approximately + 1% and finally the 3 cm one by about + 0.5%. The DD values confirm that the backscattering phenomenon for the aluminum-lead disk is confined to the first millimeters before the disk. In fact, since the DD value is normalized for the depth of the target, with the same dose increase, deep targets will have lower DD values.

PEEK-Ac disk

The PEEK-steel radiation shielding disk has a modest shielding capacity. In fact, for superficial targets, rather than shielded, the radiation is simply attenuated. The Transmission Factor at the lower surface of the disk, for each applicator, has a value of about 25% for a target of 1 cm and a value of about 13% for a target of 1.5 cm. The TF value seems to halve every 0.5 cm of target more.
For a target of 1 cm the healthy tissue at 10.5 mm, ie just where the disk starts, receives about 5 Gy of dose in the presence of the disk, an important dose value.
The backscattering phenomenon is very limited. The highest Backscattering Factor values are observed for the 1 cm target and, for the first point before the disk, it has a value of about 103% for all three applicators, then decreases very quickly. The deeper targets show practically no backscattering phenomenon. Clinical Variation values are always very small, equal to a few percentage points. Not showing a relevant backscattering phenomenon, it can be concluded that the PEEK-steel disk does not change the clinical condition of the treatment. In fact, the values found can be easily attributed to the static uncertainties of the simulations.

The Dose Difference has values of approximately 1.5% - 1.7% and approximately 1.0% - 1.3% for the 1 cm and 1.5 cm targets respectively. For the other targets the DD values are practically null.

The results obtained are in agreement with various other works present in literature [8, 10].

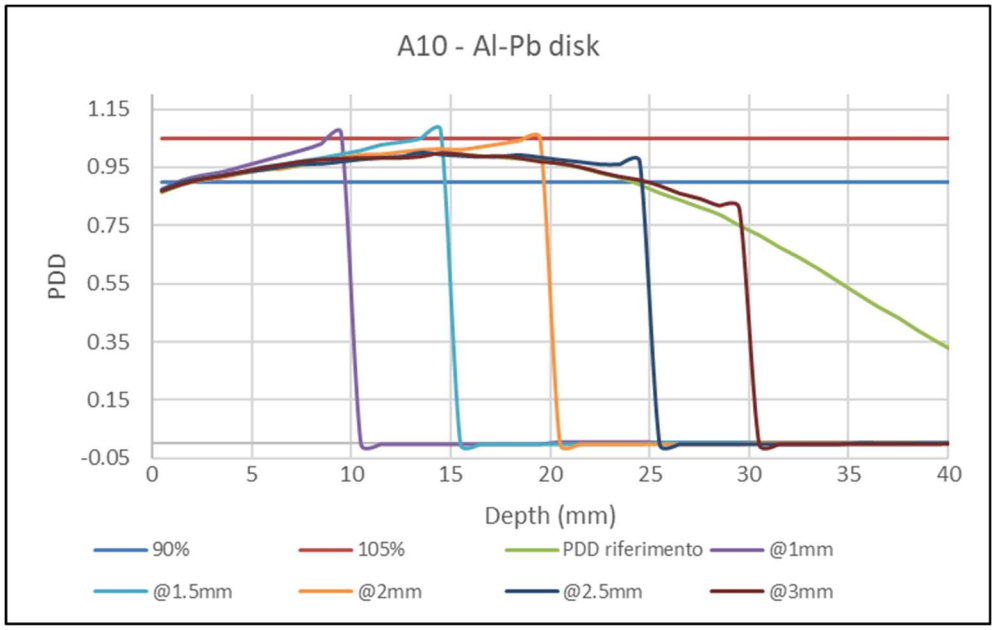

Figure 4.3 A10 Al-Pb disk PDDs for different targets

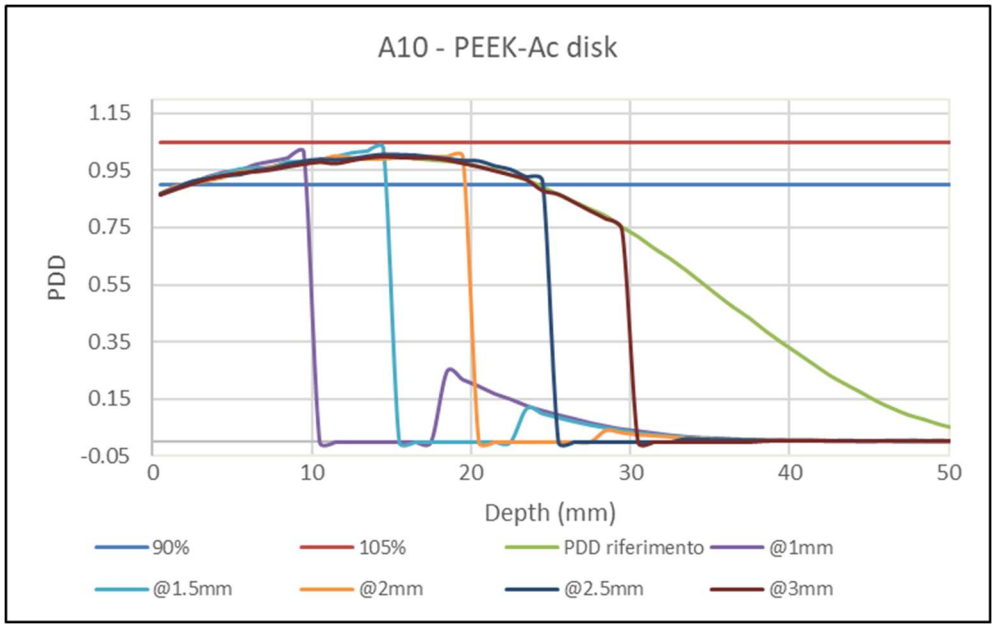

Figure 4.4 A10 PEEK-Ac disk PDDs for different targets

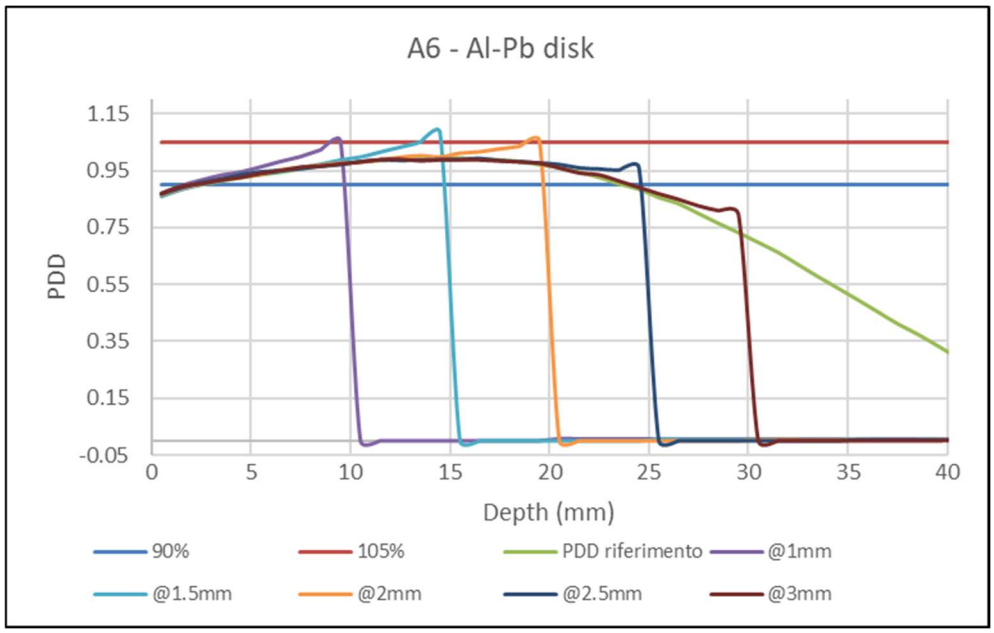

Figure 4.5 A6 Al-Pb disk PDDs for different targets

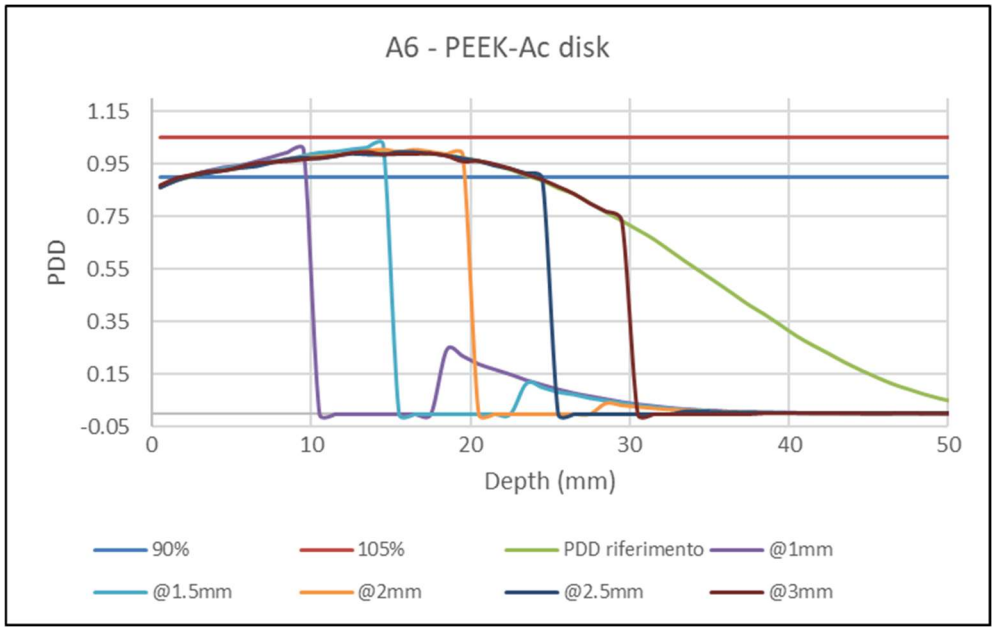

Figure 4.6 A6 PEEK-Ac disk PDDs for different targets

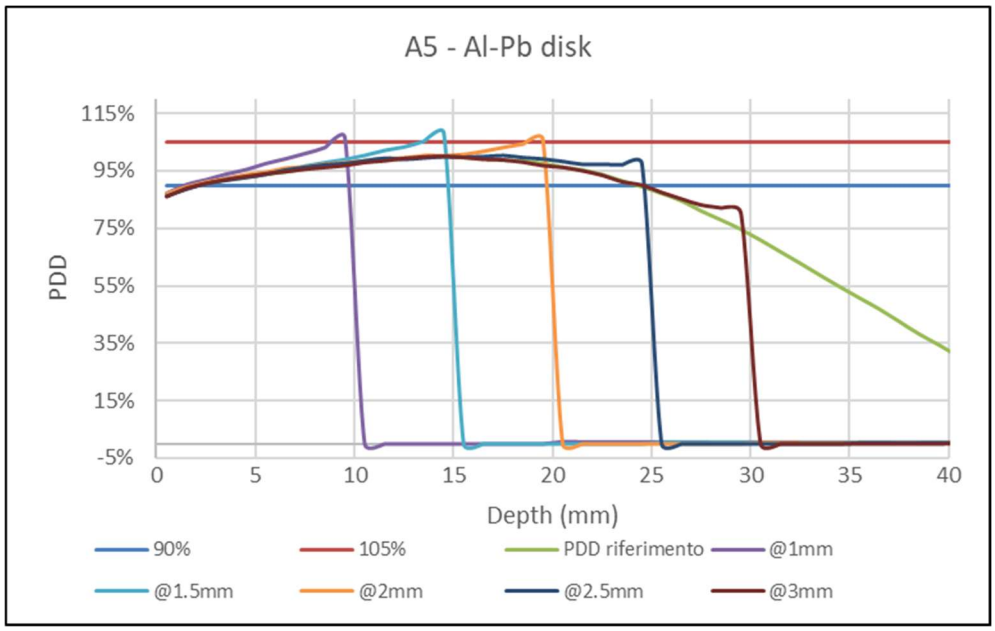

Figure 4.7 Figure 0.5 A5 Al-Pb disk PDDs for different targets

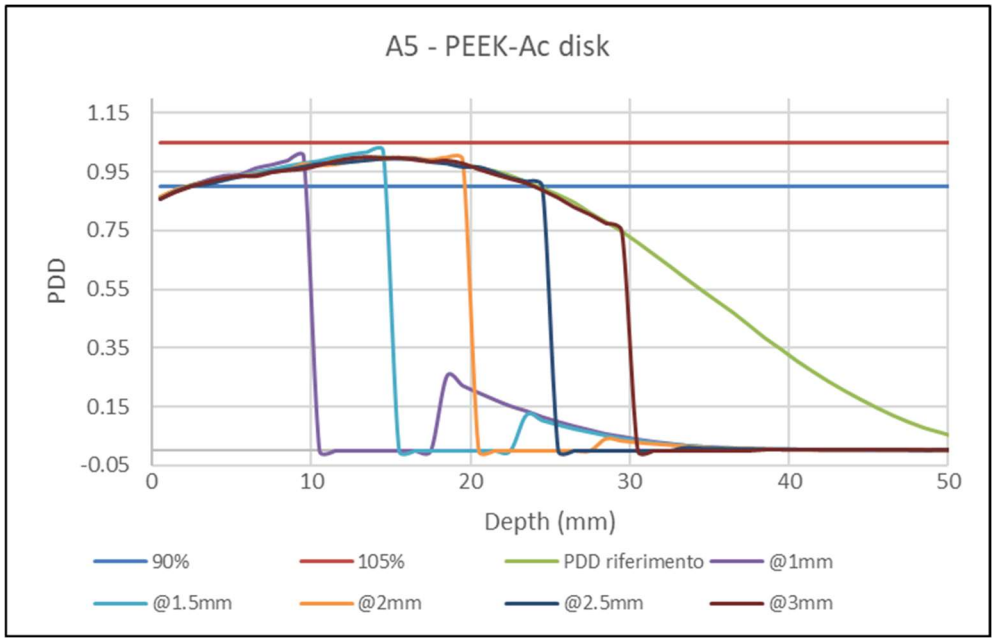

Figure 4.8 A5 PEEK-Ac disk PDDs for different targets

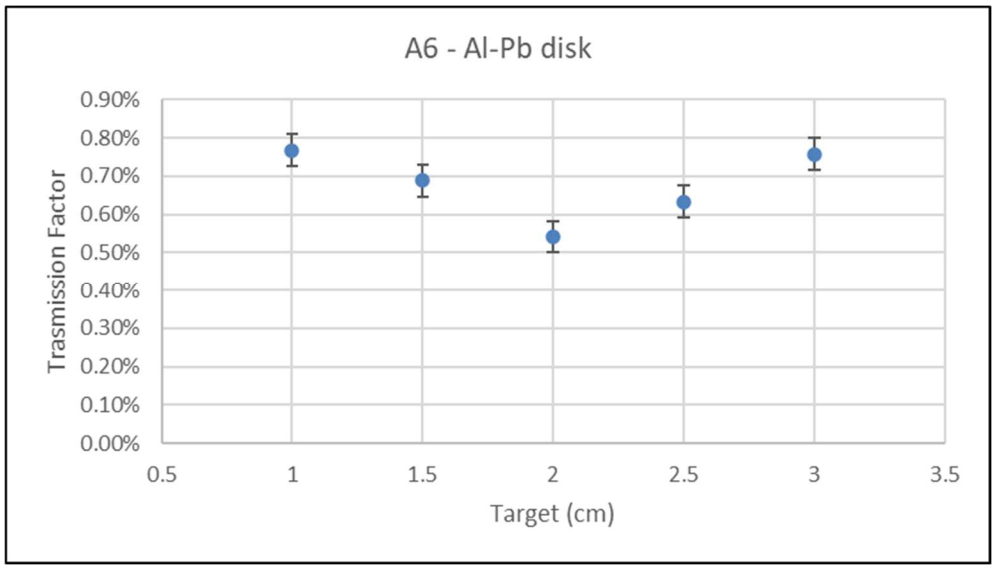

Figure 4.9 A6 Trasmission Factor for Al-Pb disk and for different targets

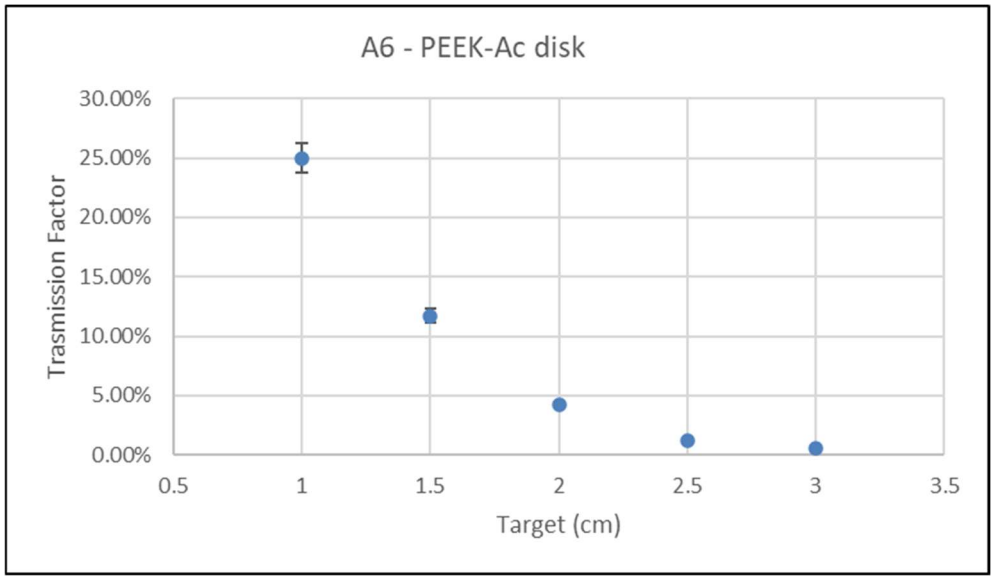

Figure 4.10 A6 Trasmission Factor for PEEK-Ac disk and for different targets

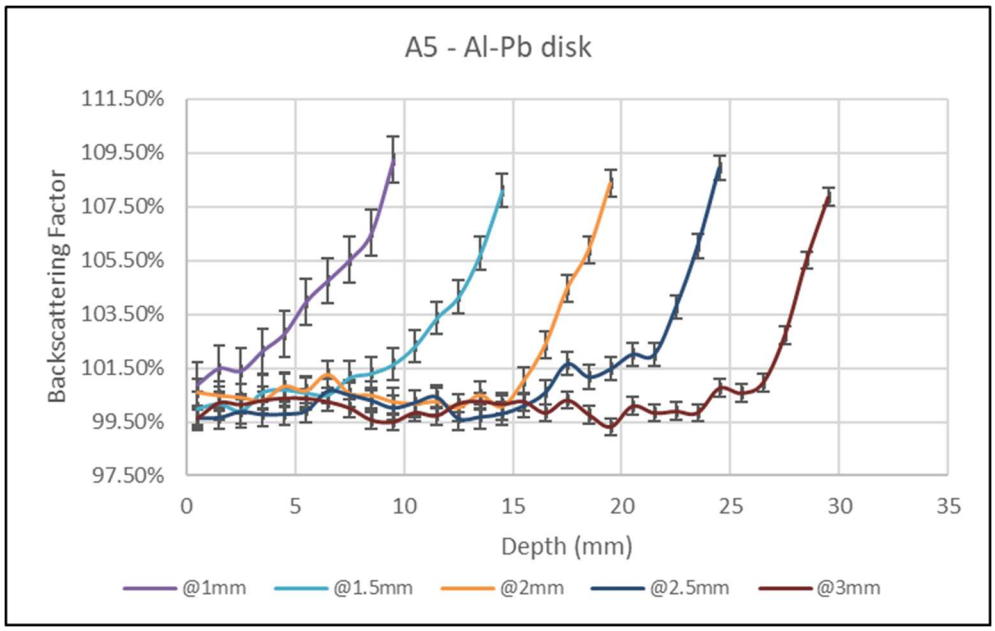

Figure 4.11 A5 Backscattering Factor for Al-Pb disk and for different targets

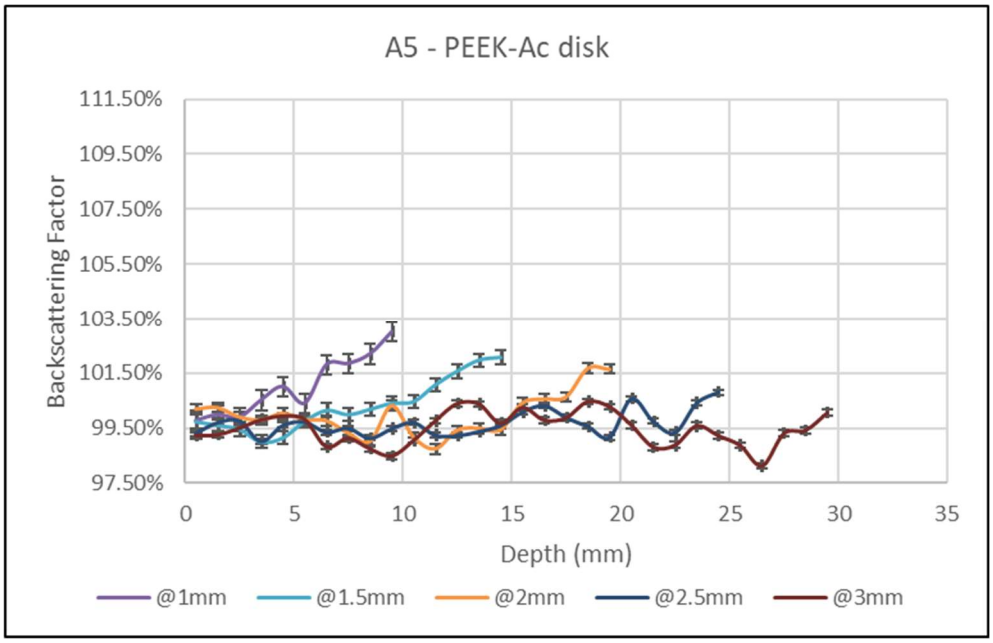

Figure 4.12 A5 Backscattering Factor for PEEK-Ac disk and for different targets

Comparison and conclusions on the use of the two different radiation shielding disks

In this paragraph the differences observed in the possible use of the two different radiation shielding disks are highlighted. It should be noted that, since the high-Z disks have different thicknesses (the lead one has a thickness of 5 mm, while the steel one is 3 mm), the considerations on the efficiency of the materials used are relative. In the last chapter the performance of the two disks with the same geometry will also be analyzed, even if these are not actually used, to evaluate the efficiency of the material.

From a clinical point of view, the PEEK-Ac disk certainly provides greater safety. Indeed, it does not substantially change the PDD, providing, especially for deep targets, a good shielding capacity of healthy tissues. In fact, it should be remembered that in clinical practice the nominal dose prescribed in the treatment plan that must be delivered to the patient does not consider either the presence of the disks or any effects of these, both positive and negative. The planning of an IOERT treatment, in which the use of a PEEK-Ac disk is used, does not provide for the risk of exceeding 105% of the nominal prescribed dose.

On the other hand, the aluminum-lead disk has excellent shielding performance for any target. The greatest difference in terms of shielding between the two disks is observed with a target of 1 cm, where the aluminum-lead disk saves the patient's tissues more than 4 Gy compared to the PEEK-steel disk for a delivered treatment in one session. However, the lead aluminum disk presents some criticalities in the target region. Presenting a more important backscattering contribution, an excess dose is observed compared to 105% of the nominal dose. It should be emphasized that the medical physicist has the possibility to correct the treatment plan a posteriori, considering the presence of this type of disk, but this is currently not accepted by national guidelines.

In general, it’s possible to conclude that the dosimetric effects generated by the presence of the radiation shielding disks does not depend significantly on the size of the applicator, since the numerical values of any parameters obtained are very similar for all the applicators if the disk used is the same.

From a physical point of view, the different physical effects in terms of radiation attenuation and backscattering can be identified in the different materials used in the construction of the disks.

As for the attenuation of radiation, lead certainly shows better performance, especially for high energy electrons. This is obviously due to a higher atomic number Z. In fact, it has a Z equal to 82, while iron, the main constituent of all types of steel, has a Z equal to 26. The composition of AISI steel 316L, used for these disks, is reported in Appendix A. It is not known whether small variations in the steel composition can change the behavior of the disks. This latter aspect may be the subject of future studies.

Furthermore, the greater attenuation capacity is justified by the greater density of lead compared to AISI 316L steel, respectively 11.34 g / cm^3 and 8 g / cm^3.

As regards the phenomenon of backscattering, this too can be justified in the first place by the higher Z of lead. Furthermore, a greater backscattering component is expected from aluminum compared to PEEK plastic, which is composed of oxygen, hydrogen and carbon [54]. The detailed atomic composition adopted in simulations is also reported in Appendix B.

The backscattering phenomenon is an elastic phenomenon. This aspect seems to justify the trend of the BF. For more superficial targets, backscattered electrons with higher energies are expected than for deep targets. In fact, it is observed that the BF trend, especially for aluminum-lead disks, takes on a steeper trend as the size of the target increases. In fact, if the backscattered electrons have a higher energy in the surface targets, these will have a greater range and will transfer energy to the tissues in a more progressive way.

It seems that PEEK plastic has a better behavior as low Z disk than aluminum due to a low backscattering phenomenon, indeed for deep targets BF values is equal to 100% for the PEEK-steel disc, i.e. no backscattering is observed. These aspects will be taken up in the next chapter.

In conclusion, the spectra of electrons and photons simulated on the rear face of the two disks are reported for a target of 1.5 cm. These are simulated with just 5 million primaries as the goal was to obtain a qualitative spectrum.

The spectra confirm the best shielding capacity of the Al-Pb disk. In fact, the fluence of electrons counted after the disk is much greater for the PEEK-Ac disk. However, from this

scoring, it is not possible to distinguish the proportion of electrons capable of passing through the disk and those that eventually are generated in it.

The photonic spectra both show a bremsstrahlung component of equal intensity, the PEEK-Ac disk however produces a significant low-energy component, with the peak around 100 keV, which also justifies the higher TF values of this disk. In the photonic spectrum of lead, the characteristic X-ray peak at 88 keV can be recognized.

The fact that the lead disk generates a lower low-energy component can be justified by a greater self-absorption phenomenon of this disk compared to the steel one.

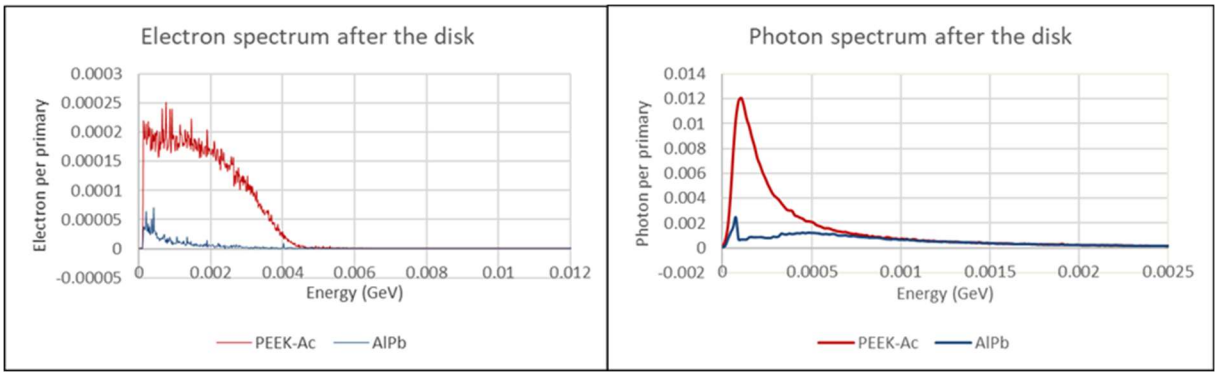

Figure 4.13 Electron and photon spectrum after the two different disks for a target of 1.5 cm

Radiation protection vest

On the market there are various radiation protection vests dedicated to health workers. In the IORT field, it was decided to adapt them to preserve the patient's skin from any diffuse radiation emitted by the applicator. Two devices were simulated: one consisting of a 0.5 mm lead layer and another consisting of an equivalent water layer 1 cm thick, representing a RT bolus. However, it must be noted that a dose component at the surface is due to radiation that actually reaches the target but is subsequently scattered (phantom scatter effect) [1]. It is therefore not shieldable by superficial devices.

The dose was evaluated on a radial coordinate perpendicular to the clinical axis of the beam (0; 0; Z) to the surface of the phantom. The cylindrical IORT irradiation geometry results in perfect azimuthal symmetry of skin exposure, of progressively lower intensity as the radial

distance from applicator wall increases. The first point of analysis is equal to the radius of the circular applicator plus 0.125 mm. The subsequent points are evaluated every 0.2 mm. In the absence of any radiation protection vest, it was observed that the skin receives a value of 2% -3% of the maximum dose in the first point closest to the applicator, moving away from the applicator the dose decreases. In confirmation of what has already been described in the "Validation" chapter, the 10 cm circular applicator has a higher dose to the skin than the 6 cm and 5 cm circular applicators, which have similar dose values. In the case of an IORT treatment delivered in a single session with a nominal dose of 20 Gy, the patient receives a maximum dose value between 0.4 Gy and 0.6 Gy based on the applicator used.
The water equivalent bolus has a greater shielding capacity than the lead apron.
The Transmission Factor, in this case given simply by the dose ratio in the presence of the radiation protection vests and in reference conditions, was calculated along the entire radial coordinate. The results obtained are reported in *Figure 4.12*.
The TF trend seems to confirm that a component of scattered radiation coming from the target. In fact, for the first millimeters around the applicator, the TF shows fairly high values for both devices between 60% and 80%. Moving away from the applicator, the TF value decreases. Indeed moving away from the applicator, it is expected that the ratio between dose diffused by the applicator - dose scattered by the target increases due to the lower attenuation of the radiation by air compared to that of the water.
Aprons aren't actually that useful. Given a nominal dose of 20 Gy for the treatment, the saving in dose to the skin is between 0.05 Gy and 0.15 Gy based on the distance from the applicator.
The analysis of the energy spectra of electrons and photons between the bolus and the water phantom confirm that the water equivalent bolus has a better ability to attenuate the radiation, especially reducing the high energy component of electrons. Both radiation protection vests, however, increase the photonic component compared to the case in which these are not present. However, the lead apron produces a higher energy photonic component. The energy spectra shown in *Figure 4.13* refer to the 10 cm circular applicator, those of 6cm and 5cm have practically the same trends.

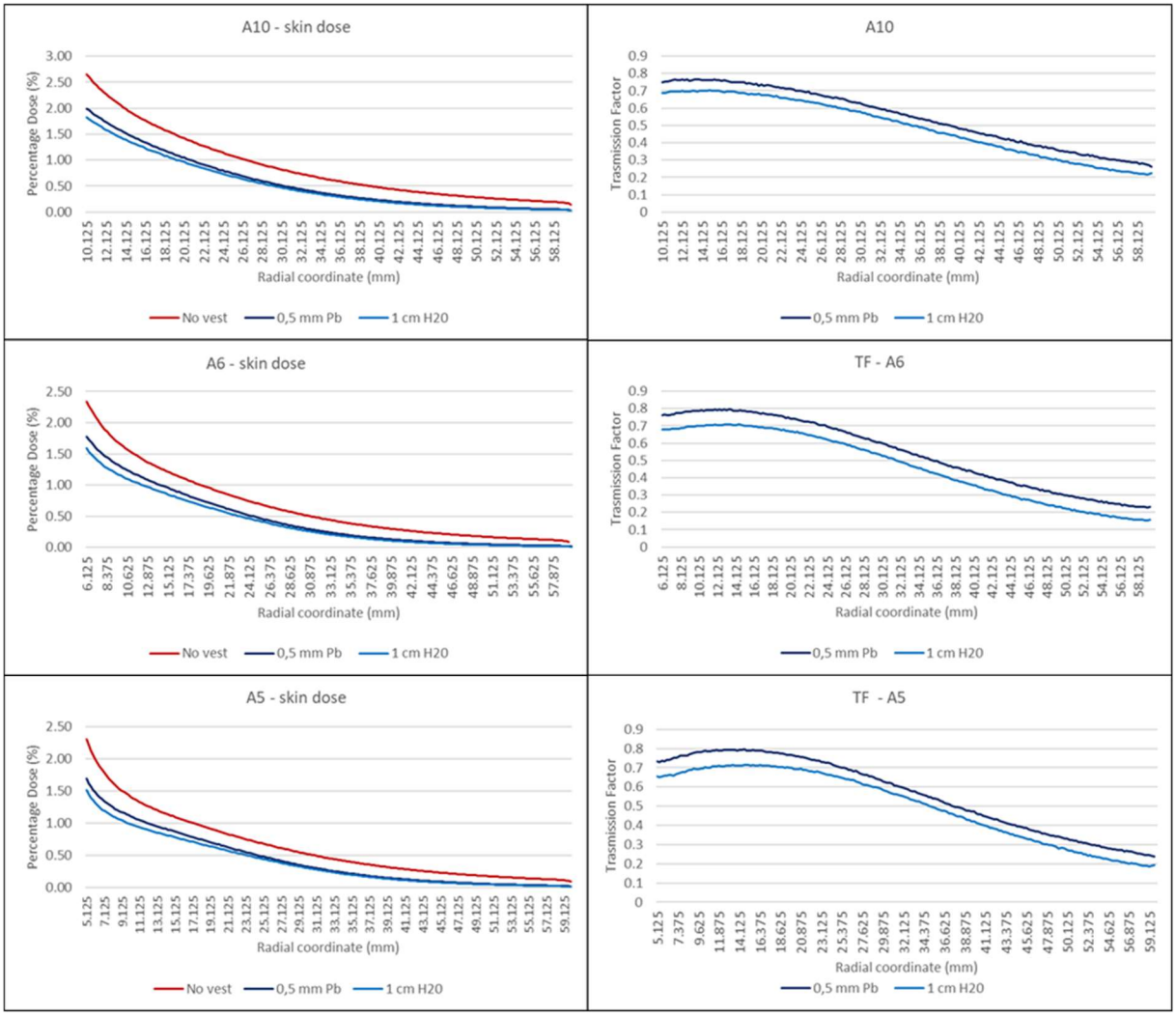

Figure 4.144 Percentage dose (right) at the phantom and TF (left) for A10, A6 and A5

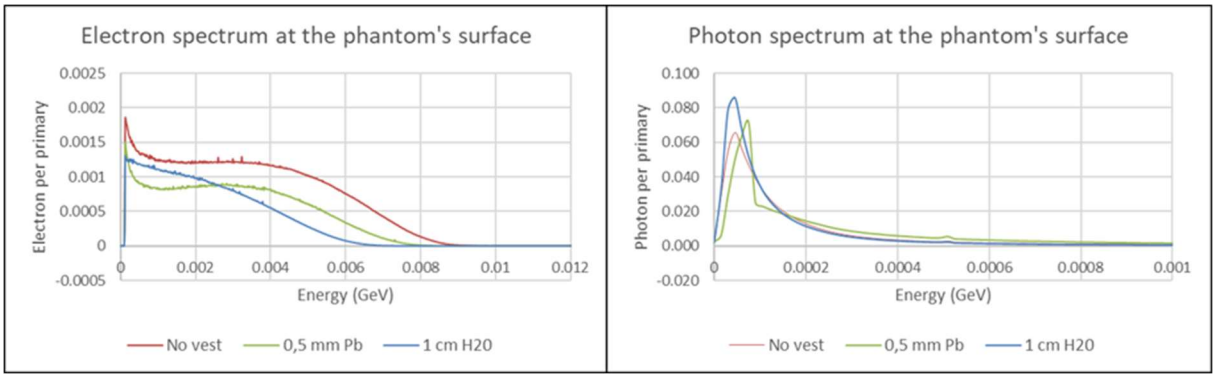

Figure 4.15 Electron and photon spectrum evaluated after the vest and before the phantom

Applicator bolus

The experimental measurements made for the circular applicators of 5, 6 and 10 cm with a nominal energy of 10 MeV show PDD over 90% already from the first millimeters. It follows that, at least for this energy and these applicators, the applicator bolus will be not used with the aim of increasing the dose in the surface of the target.

On the other hand the PDDs for the same applicators at a nominal energy of 8 MeV do not reach the 90% of the maximum dose in the first millimeters. In this case, an applicator bolus could be exploited to reach the 90% isodose already in this region.

However, it should be emphasized that in the clinical condition, the nominal energy of 10 MeV is the most used with the possibility to "model" the irradiation field with the use of radiation shielding disk and applicator bolus.

The applicator bolus is in any case used to avoid herniation tissue phenomenon and to uniform the irradiation field transversally for any applicator and for any nominal energy.

The aim of the simulations performed with the bolus was to verify that PMMA, a water-equivalent material, does not modify the shape of the PDD. Only a rigid translation of the PDD proportional to the bolus thickness is expected.

First, it was decided to simulate the use of a 10 mm thick bolus with a 10 cm circular applicator and with a nominal energy of 10 MeV. The results, shown in *Figure 4.14*, confirm what was expected. In fact, a rigid translation of 10 millimeters is observed, precisely equal to the thickness of the bolus, of the PDD with bolus compared to that in reference conditions. The two simulations are obtained with different seeds to be statistical independent. By performing a Gamma Test between the PDD with bolus and that in the reference condition, the latter evaluated from the eleventh millimeter onwards, it is observed that the test is passed with parameters of 0.1% and 0.1 millimeter. It is therefore confirmed that the use of bolus, given its water-equivalent composition, does not change the shape of the PDD, but only imposes a rigid leftward translation equal to its thickness.

In conclusion it was decided to simulate the use of two bolus, respectively 5 and 10 millimeters, in the presence of an aluminum-lead radiation shielding disk placed at a depth of 2 cm. As can

be seen from *Figure 4.16*, the use of the 5 mm bolus generates an almost flat PDD thanks also to the backscattering phenomenon induced by the disk. On the contrary, the use of a 10 mm bolus tends to shift the PDD too much, generating a target region that does not reach the 90% isodose also in presence of the backscattering phenomenon induced by the disk.

The applicator bolus can therefore be exploited to uniform the irradiation field both transversely and axially if coupled to a disk.

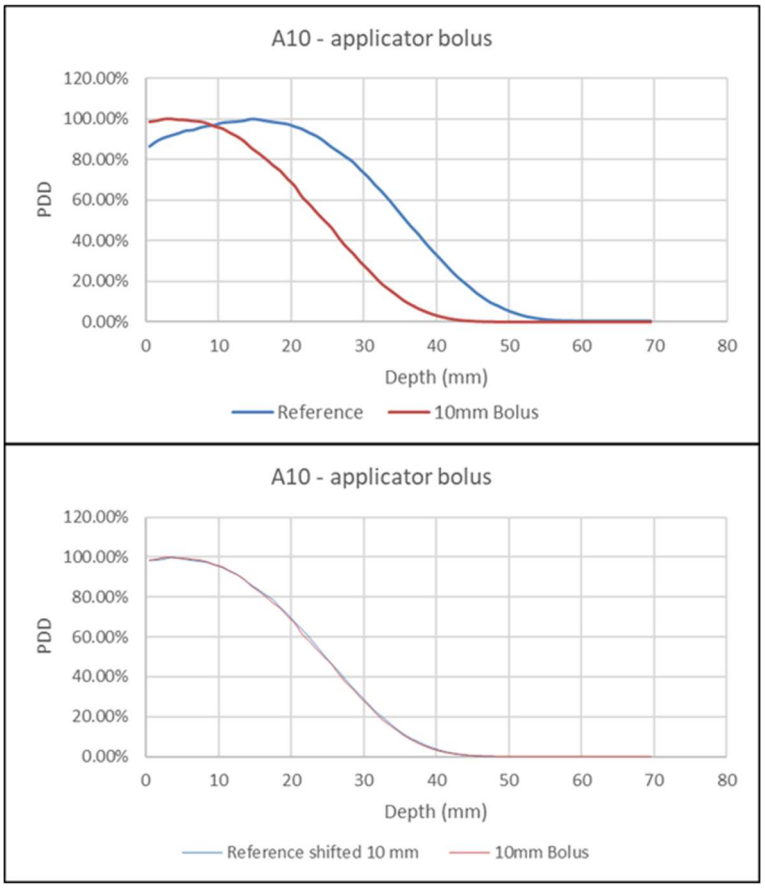

Figure 4.15 In the graph above the reference condition and the simulation with the bolus are represented both for A10. In the graph down the latter and the reference condition, evaluated from the eleventh millimeter onwards, are shown to underling that the shape do not change with the use of a bolus.

Furthermore, it can be exploited for superficial targets to avoid an excessively harmful disk-induced backscattering phenomenon. As already highlighted in the previous paragraphs, in fact, the build up for an energy of 10 MeV is around 15 mm deep, if a radiation shielding disk is placed at this depth the greatest backscattering effect and the possibility of exceeding the

isodose of the 105% are expected. With the use of a bolus, this problem could be avoided by shifting the build up point to shallower depths.

In future works it could be interesting to develop this aspect, studying the best couplings between bolus and radiation shielding disk for various thicknesses and various depths.

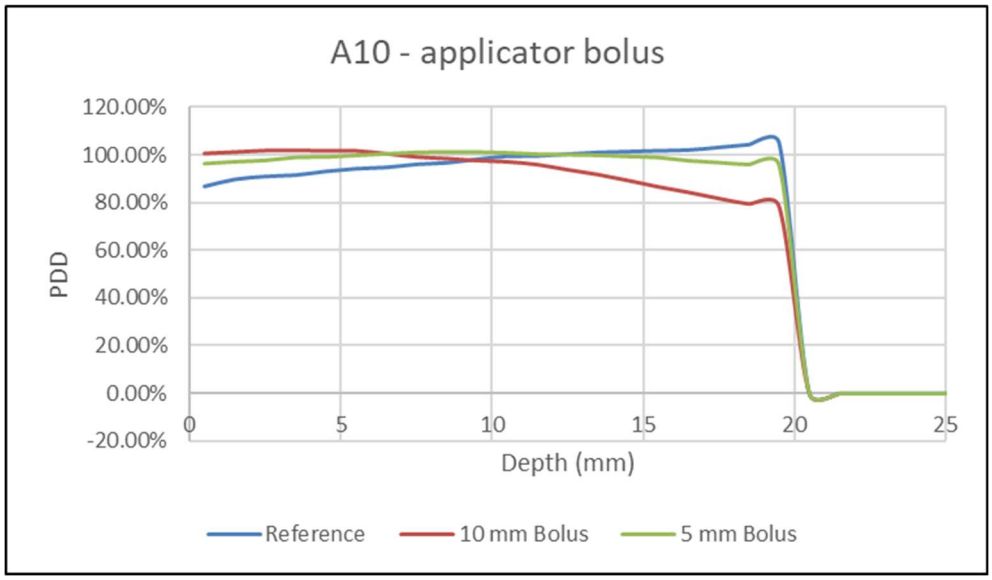

Figure 4.16 PDDs for A10 with a AlPb disk at 2 cm depth with a 10mm bolus, a 5mm bolus and without

Chapter 5

Possible improvement for radiation shielding disks

In the previous chapter, a complete characterization of the dosimetric variations induced by the presence of the radiation shielding disks in use at the ASST Papa Giovanni XXIII (Bergamo) hospital was presented. The criticalities of these were also highlighted: the aluminum-lead disk generates important backscattering phenomenon, on the contrary the PEEK-steel disk has a modest shielding capacity for thin targets.

The aim of this chapter is to first investigate the properties of the individual layers of the disks, in order to better understand the critical issues that have emerged. Four different 5mm thick layers of aluminum, lead, steel and PEEK were individually simulated at a depth of 1.5cm. This dimension of the target was chosen because the build-up of the PDD is observed at this depth and is therefore the most critical condition.

Finally, some variations of the geometry of the layers of the disks in use were studied to try to correct any critical issues that emerged. In fact, in the literature there are already various studies on the materials of the radiation shielding disks and on the variations of these to the dose profiles [8, 9, 10, 54]. They all agree that the choice of aluminum-lead and plastic-steel guarantees the best results. Trying to fill some critical issues of these, the thicknesses of the layers of the disks has been varied. The following cases were studied:

- Increase the steel layer for surficial targets to study the possible increase in the radiation shielding capacity.
- Reduce the lead layer to see if it affects the backscattering phenomenon.
- Coupling a layer in PEEK and one in lead with different thicknesses to observe the variation of the backscattering phenomenon.

– Reduce the aluminum layer for target of 3 cm to observe the variation of the backscattering phenomenon and possibly exploit its increase in order to achieve 90% isodose for the whole target.

It is emphasized again that the objective of this thesis is the characterization of the various devices, currently in use at the ASST Papa Giovanni XXIII (Bergamo). These last considerations on the variation of the geometry of the layers of the disks are therefore just a starting point for future works and possible improvements to develop "ad hoc" geometry of the radiation shielding disks for every dimension of the target.

Analysis of single layer disk

High Z layers

The analysis on the high Z single-layer disks is conducted by simulating a lead disk and an AISI 316L steel disk, both 5 mm thick, for a 1.5 cm target.

It results that the steel disk has better performance than the lead one. In fact, it has a comparable shielding capacity, quantifiable with a Transmission Factor equal to 1.90% ± 0.04% for the steel one and 1.09% ± 0.05% for the lead one.

On the other hand, the backscattering phenomenon is much more important in the lead one. In fact, if we compare the Backscattering Factor of the two different disks at a depth of 14.5 mm, it is equal to 118.44% ± 0.60% for the steel one and 142.66% ± 0.51% for the lead one. The trend of the BF is shown in *Figure 5.2*.

From this last observation it is clear why it is necessary to couple a lead layer with an aluminum one. The latter one in fact has a greater radiation's attenuation capacity than PEEK plastic, as it will be shown in the next paragraph.

The results obtained are in agreement with other works in literature [54].

It can be concluded that, for the same geometry, the AISI 316L steel disk as a high Z layer is preferable.

As already suggested in the previous chapter, this conclusion is limited to this type of steel, in fact It is not known whether small variations in the steel composition can change the behavior of the disks.

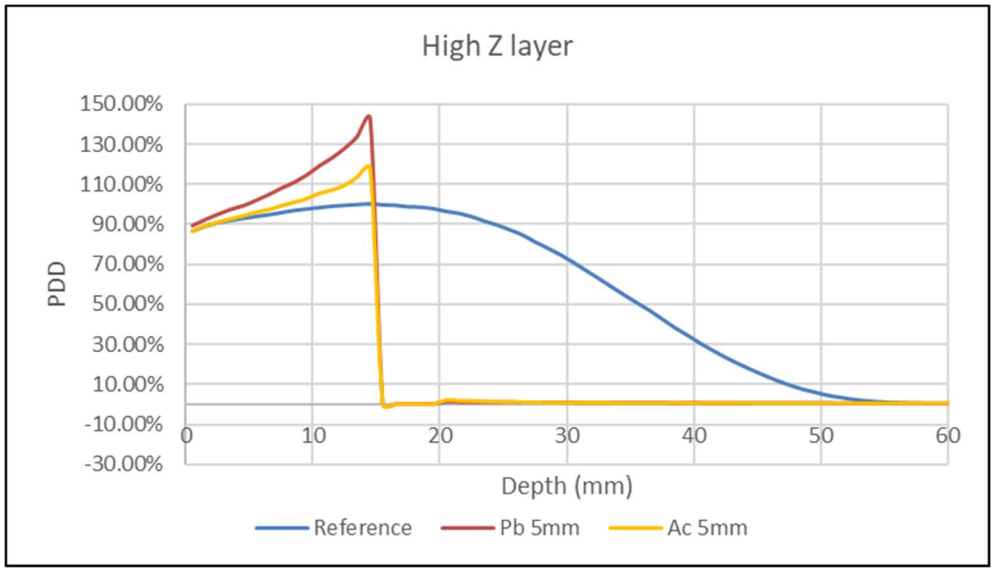

Figure 5.1 High Z layer PDDs for a 1.5 cm target

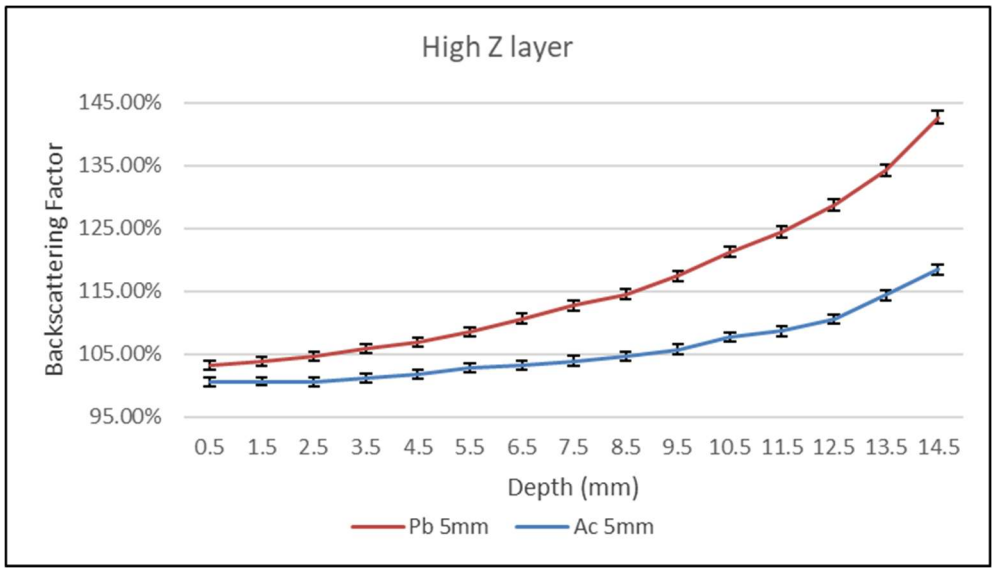

Figure 5.2 High Z layer Backscattering Factors for a 1.5 cm target

Low Z layers

The analysis on the low Z single-layer disk is conducted by simulating a PEEK disk and an aluminum disk, both 5 mm thick and at 1.5 cm depth.

PEEK is a plastic material slightly denser than PMMA (the characteristics of these two materials are shown in Appendix A). Indeed, no backscattering phenomenon are observed, but at the same time its attenuation is only slightly greater than that of a water-equivalent material such as PMMA. In fact, as can be seen from the *Figure 5.3*, in which the PDDs with the two low Z single-layer disks are shown, the presence of a PEEK disk practically does not change the trend of the PDD in the region posterior to the disk.

On the contrary, aluminum has a better ability to attenuate radiation, in fact it presents a Transmission Factor of 83.61% ± 0.17%. However, it also has a significant backscattering contribution. As shown in the *Figure 5.4*, it is comparable with that of the Al-Pb disk placed at the same depth.

It can therefore be concluded that the excessive backscattering contribution of the Al-Pb disk is due exclusively to the aluminum layer, although this is necessary to attenuate the important backscattering phenomenon of the lead one.

Also these results are in agreement with works present in literature [54].

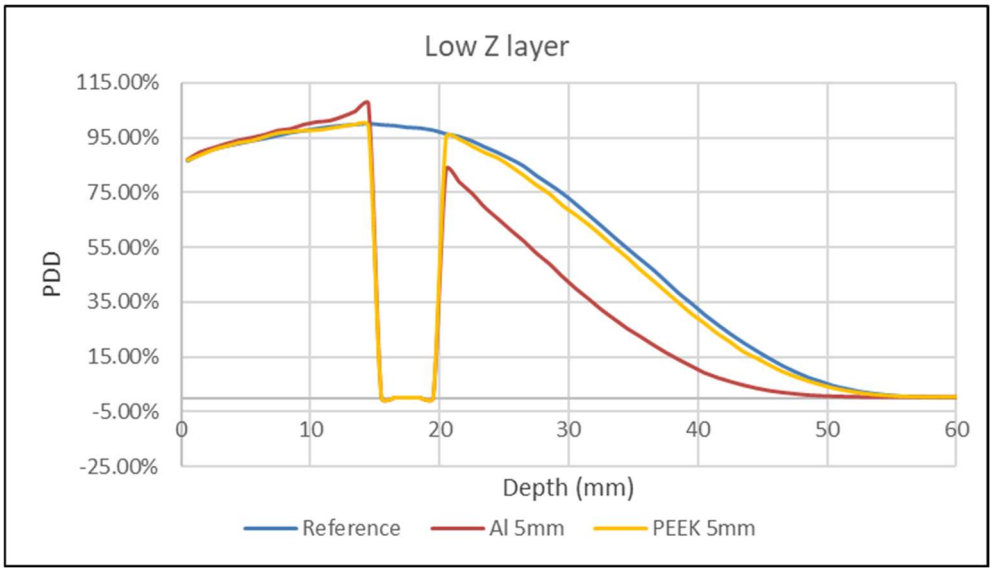

Figure 5.3 Low Z layer PDDs for a 1.5 cm target

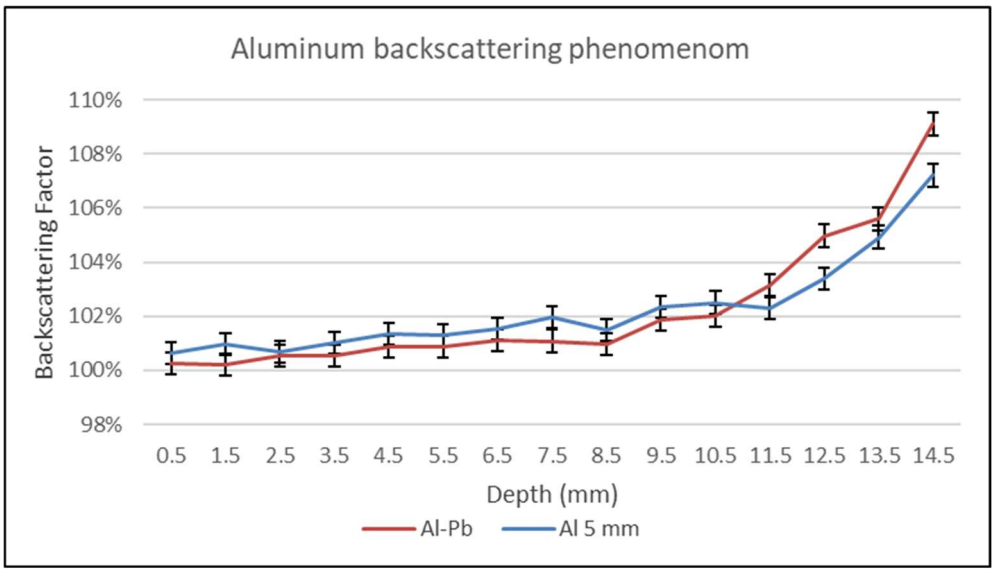

Figure 5.4 Aluminum backscattering phenomenon for a 1.5 cm target

Thicknesses variation of the layers of the disks

Steel thickness variation in the PEEK-Ac disk

Observing the conclusions drawn in the previous paragraph it was decided to increase the thickness of the steel layer of the PEEK-Ac disk to see the response of a radiation shielding disk with the same geometry as the one in Al-Pb. The goal is to try to see if it is possible to improve the shielding capacity of the PEEK-Ac disk.

For this purpose, two PEEK-Ac disks with steel layers respectively 4 mm and 5 mm thick were simulated. It was decided to simulate a target of 1 cm, since it is the one for which the greater fluence and the greater average energy of the primary electrons are expected.

The 4 mm steel layer has a Transmission Factor equal to 6.33% ± 0.15%, while the 5 mm equal to 1.58% ± 0.10%.

On the other hand, the backscattering phenomenon does not vary changing the steel thickness, as evidenced by the *Figure 5.5*.

It can be concluded that, given two radiation shielding disks, one in Al-Pb and one in PEEK-Ac, both 1 cm thick, these have a comparable capability of radiation's attenuation. The second one, however, does not change the clinical condition of the treatment and therefore could be preferable.

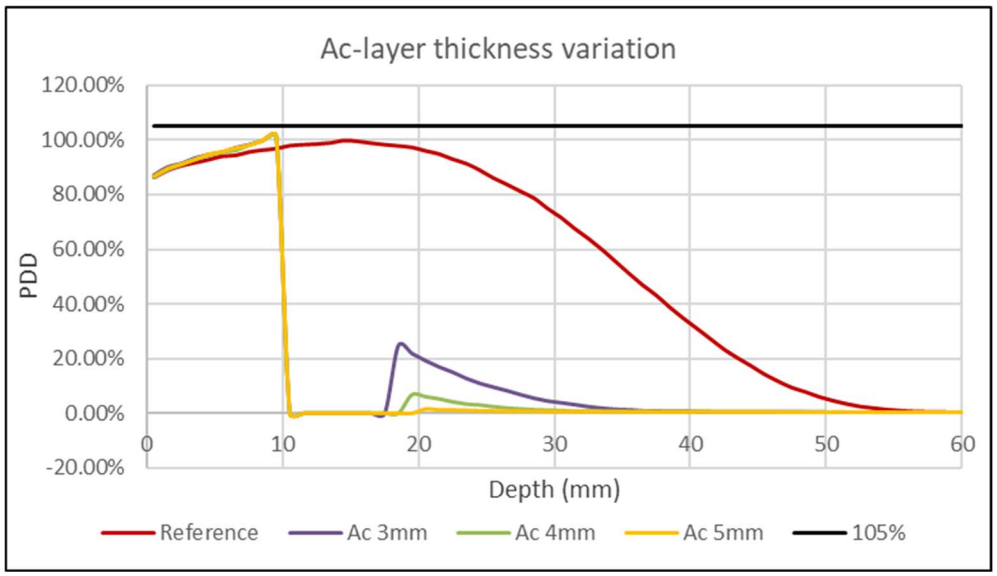

Figure 5.5 Different steel layer thicknesses PEEK-Ac disks PDDs for a 1 cm target

Lead thickness variation in the Al-Pb disk

It is tried to vary the lead thickness to see if this influenced the backscattering phenomenon in any way. Two Al-Pb disks with lead layers of 4 mm and 3 mm respectively are simulated at a depth of 1.5 cm, since this is where the backscattering phenomenon is most observed. Compared to the Al-Pb disk with a 5 mm lead layer, no variation is observed either in terms of backscattering or in terms of radiation attenuation by reducing the lead thickness to 3mm.

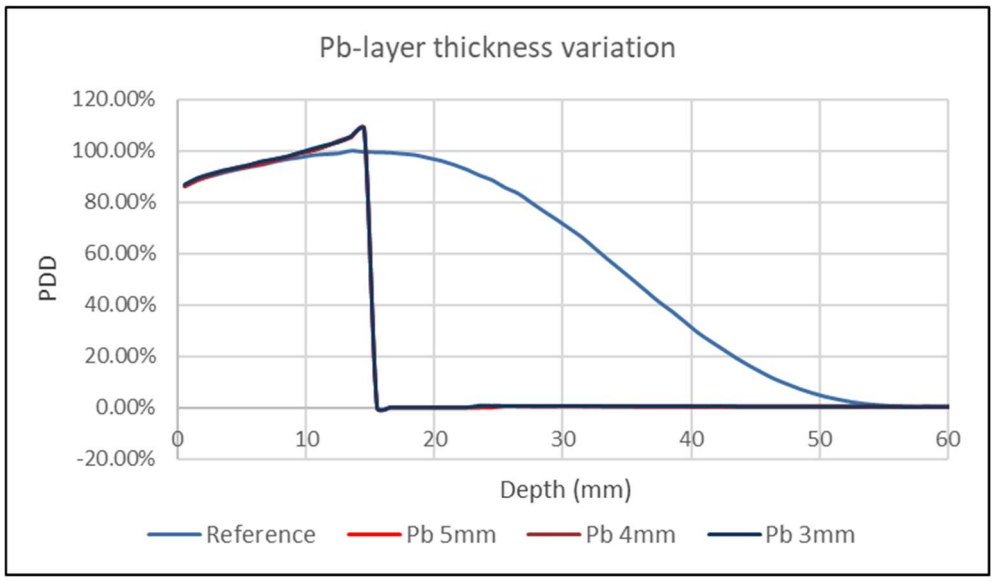

Figure 5.6 Different lead layer thicknesses Al-Pb disks PDDs for a 1.5 target

PEEK-Pb disk

Observing the result illustrated in the last paragraph, which seems to underline an excess thickness of the lead layer, it was decided to try to simulate a PEEK-Pb disk. Without exceeding the 1 cm thickness limit for the entire radiation shielding disk, the lead layer was progressively reduced to increase the PEEK layer. Two disks were simulated, one of 7 mm in PEEK and 3 mm of lead and another of 8 mm of PEEK and 2 mm of lead, at a depth of 1.5 cm. Both have better radiation attenuation capacity than the PEEK-Ac disk (5mm - 3mm). In particular, the first has a Transmission Factor equal to 0.86% ± 0.06%, while the second equal to 3.09 ± 0.07%. The backscattering phenomenon, as shown in the *Figure 5.7*, is less for both than in the Al-Pb disk (5mm - 5mm).

The disk with a layer of 7 mm in PEEK imposes at maximum a PDD of 105.56% ± 0.17%, therefore slightly higher than the isodose limit of 105%. Having studied this last disk at a depth of 1.5 cm, i.e. near the build up point where the maximum backscattering phenomenon is expected, it can be concluded that for all other targets there should be no risk of exceeding the isodose limit of 105%.

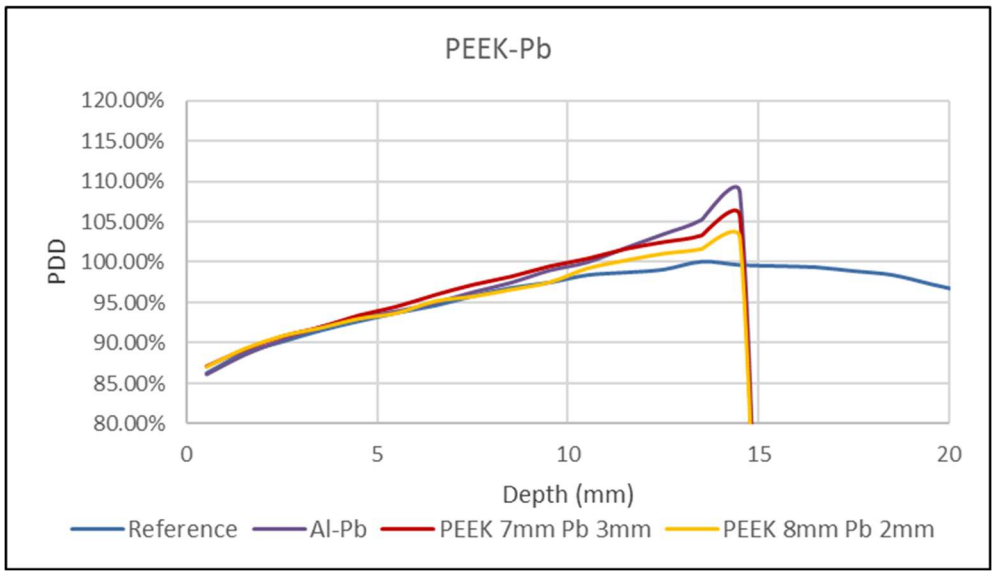

Figure 5.7 Two different 1 cm thickness PEEK-Pb disks PDDs compared to the Al-Pb (5mm – 5mm) PDD

In these last paragraphs, two possible alternatives to the disks in use at the ASST Papa Giovanni XXIII (Bergamo) hospital have been highlighted. PEEK-Steel disk (5mm -5mm) or PEEK-Pb disk (7mm - 3mm) have a radiation shielding capacity comparable to Al-Pb disk (5mm - 5mm). At the same time, they present much smaller backscattering phenomenon.
Finally, one could think of using an ultra-dense plastic as a low-Z disk, loaded for example with lead oxide or other oxides [59,60]. These should have the advantage of guaranteeing the zero-backscattering characteristic of plastic material but have a better attenuation capacity than PEEK plastic. An in-depth study that starts from these last considerations could lead to the construction of a radiation shielding disk with an ability to shield the primary radiation, which at the same time does not change the clinical condition of irradiation.

Aluminum thickness variation in Al-Pb disk

It is tried to reduce the aluminum layer to increase the backscattering phenomenon and try, for a target of 3 cm, to increase the dose region that falls within the 90% -105% isodose range. Four different disks were simulated by progressively reducing the aluminum layer from 4 mm to 1 mm.

As can be seen from the *Figure 5.8*, only the 1 mm layer disk allows to reach the 90% isodose in the first millimeter before the disk. However, having a very low energy, the backscattered electrons are not able to cover all the range necessary to impose a dose greater than 90% on the whole target.

It follows that an improvement in the dose coverage of the target is observed with this last disk, but it's not enough. In future works, ad hoc disks could be studied for the irradiation of targets greater than 2.5 cm, exploiting the backscattering phenomenon induced by these in such a way as to adequately irradiate the whole target. In particular it will be necessary to focus on the energy spectrum of the backscattered electrons to understand the range that these are able to cover.

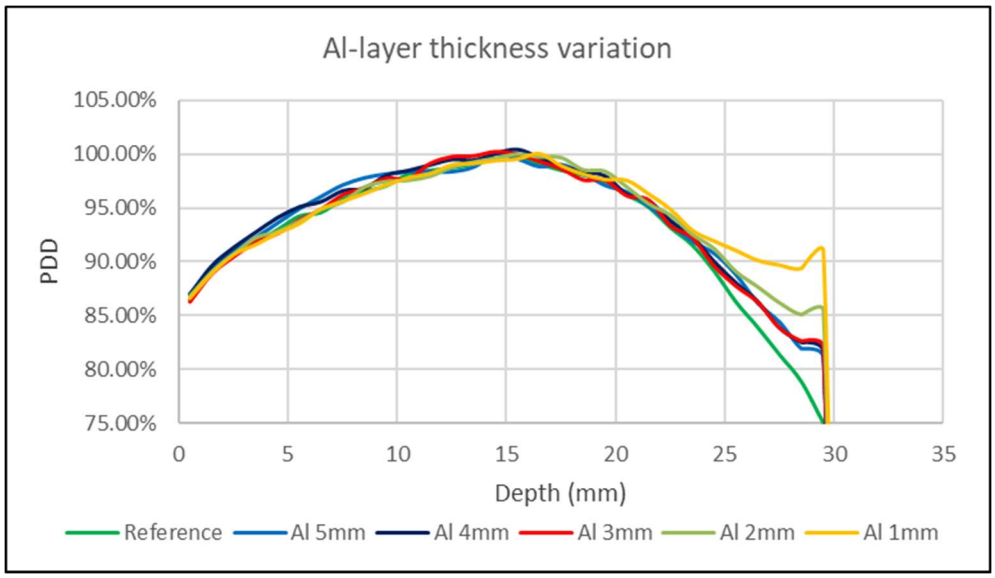

Figure 5.8 5 Different aluminum layer thicknesses Al-Pb disks PDDs for a 1 cm target

Conclusions and final remarks

The thesis proposes a complete dosimetric characterization of a IORT treatment performed with a LINAC Novac-11 and the various associated devices, used at the ASST Papa Giovanni XXIII (Bergamo) hospital.

First of all the FLUKA code was validated for a delivery with nominal energy of 10 MeV, describing the energy spectrum of the primary electrons for three different circular applicators with a diameter of 10, 6 and 5 cm. An excellent agreement was found between the PDD measured experimentally and that obtained through the FLUKA simulations.

The main result obtained underlines the usefulness of both radiation shielding disks in preserving healthy tissues posterior to the target. However, the criticalities of these were also highlighted: the aluminum-lead disk generates important backscattering phenomenon, on the contrary the PEEK-steel disk has a modest shielding capacity for thin targets. In the last chapter some improvements are proposed, as increasing the steel layer or a PEEK-lead disk. Finally, also the use of a ultra-dense plastic loaded with oxides are suggested as material for low Z disk. These last setups could be developed in future works.

The total amount of dose received by the skin around the applicator was evaluated and the positive effect induced by the use of two different radiation protection vests was quantified. In particular it was underlined the relation between the dimension of the applicator and the leakage radiation.

Finally, the effect of the presence of a PMMA applicator bolus was evaluated, underling as this device does not change the dose profile but just impose a rigid translation of it. It was also underlined the potential to couple applicator bolus and radiation shielding disk for various targets thicknesses in order to obtain a flat dose profile in the target region. This last concept could also be an aspect to develop in future works.

Appendix A

Compositions of the materials that make up the radiation shielding disks

The compositions of steel (AISI 316L), PEEK plastic (polyether-ether-ketone) and PMMA (polymethylmethacrylate) are reported. The lead disk is made from pure lead.

Material	Element	Atomic ratio
PMMA Density 1.18 g cm^{-3}	H C O	8 5 2
PEEK Density 1.3 g cm^{-3}	H C O	12 19 3

Table 2 Composition plastic material

Material	Element	Weigh fraction
AISI 316L Density 8 g cm^{-3}	Fe Cr Ni Mo Mn Si P C S N	67.15% 17.50% 11.50% 2.25% 1.00% 0.50% 0.20% 0.15% 0.15% 0.50%

Table 3 AISI 316L Steel composition

Appendix B

Numerical results of simulation in presence of radiation shielding disks

The numerical results of the simulations of the circular applicators with 10, 6 and 5 cm diameter in the presence of the radiation shielding disks at a nominal energy of 10 MeV are reported.
The simulations are performed with targets of 1mm, 1.5mm, 2mm, 2.5mm and 3mm.

A10 – Al-Pb									
Target 10 mm		Target 15 mm		Target 20 mm		Target 25 mm		Target 30 mm	
BF @6.5	104.68%±0.58%	BF @11.5	104.84%±0.56%	BF @16.5	103.08%±0.58%	BF @21.5	102.05%±0.57%	BF @26.5	102.73%±0.64%
BF @7.5	105.26%±0.57%	BF @12.5	105.13%±0.50%	BF @17.5	104.74%±0.61%	BF @22.5	103.29%±0.54%	BF @27.5	103.76%±0.64%
BF @8.5	106.82%±0.57%	BF @13.5	105.98%±0.55%	BF @18.5	106.41%±0.63%	BF @23.5	105.08%±0.71%	BF @28.5	103.93%±0.61%
BF @9.5	110.00%±0.59%	BF @14.5	107.93%±0.51%	BF @19.5	107.78%±0.57%	BF @24.5	109.03%±0.58%	BF @29.5	108.14%±0.70%
TF @10.5	0.77%±0.04%	TF @15.5	0.60%±0.04%	TF @20.5	0.42%±0.05%	TF @25.5	0.45%±0.06%	TF @30.5	0.46%±0.10%
DD	3.65%±0.75%	DD	2.56%±0.77%	DD	1.66%±0.75%	DD	1.03%±0.75%	DD	0.92%±0.78%
DIFF	-3.00%	DIFF	-7.00%	DIFF	-1.50%	DIFF	5.60%	DIFF	4.00%

Table 4 Numerical result A10 / Al-Pb

A6 – Al-Pb									
Target 10 mm		Target 15 mm		Target 20 mm		Target 25 mm		Target 30 mm	
BF @6.5	103.86%±0.36%	BF @11.5	103.12%±0.36%	BF @16.5	102.29%±0.42%	BF @21.5	101.55%±0.41%	BF @26.5	101.76%±0.57%
BF @7.5	104.35%±0.49%	BF @12.5	104.47%±0.56%	BF @17.5	103.84%±0.38%	BF @22.5	103.15%±0.47%	BF @27.5	103.28%±0.56%
BF @8.5	105.68%±0.42%	BF @13.5	105.23%±0.39%	BF @18.5	105.27%±0.34%	BF @23.5	105.30%±0.50%	BF @28.5	105.77%±0.43%
BF @9.5	107.98%±0.42%	BF @14.5	109.00%±0.44%	BF @19.5	108.36%±0.44%	BF @24.5	108.49%±0.54%	BF @29.5	108.76%±0.57%
TF @10.5	0.75%±0.04%	TF @15.5	0.59%±0.04%	TF @20.5	0.39%±0.03%	TF @25.5	0.37%±0.04%	TF @30.5	0.32%±0.05%
DD	3.09%±0.58%	DD	1.83%±0.57%	DD	1.20%±0.58%	DD	0.81%±0.59%	DD	0.58%±0.60%
DIFF	1%	DIFF	-10%	DIFF	-2.50%	DIFF	8.00%	DIFF	2.00%

Table 5 Numerical result A6 / Al-Pb

A5 – Al-Pb									
Target 10 mm		Target 15 mm		Target 20 mm		Target 25 mm		Target 30 mm	
BF @6.5	104.75%±0.46%	BF @11.5	103.36%±0.45%	BF @16.5	102.37±0.40%	BF @21.5	102.00%±0.40%	BF @26.5	100.95%±0.57%
BF @7.5	105.52%±0.46%	BF @12.5	104.16%±0.42%	BF @17.5	104.44%±0.39%	BF @22.5	103.76%±0.40%	BF @27.5	102.71%±0.53%
BF @8.5	106.54%±0.35%	BF @13.5	105.72%±0.40%	BF @18.5	105.89%±0.41%	BF @23.5	106.03%±0.40%	BF @28.5	105.50%±0.51%
BF @9.5	109.25%±0.41%	BF @14.5	108.19%±0.33%	BF @19.5	108.37%±0.43%	BF @24.5	108.94%±0.46%	BF @29.5	107.85%±0.56%
TF @10.5	0.81%±0.03%	TF @15.5	0.59%±0.04%	TF @20.5	0.46%±0.04%	TF @25.5	0.35%±0.05%	TF @30.5	0.36%±0.06%
DD	3.66%±0.60%	DD	1.99%±0.58%	DD	1.41%±0.56%	DD	1.03%±0.56%	DD	0.47%±0.58%
DIFF	-3.00%	DIFF	-11.00%	DIFF	-4.00%	DIFF	3.00%	DIFF	2.00%

Table 6 Numerical result A5 / Al-Pb

A10 - PEEK-Ac									
Target 10 mm		Target 15 mm		Target 20 mm		Target 25 mm		Target 30 mm	
BF @6.5	102.87%±0.58%	BF @11.5	101.45%±0.65%	BF @16.5	100.45%±0.53%	BF @21.5	101.43%±0.59%	BF @26.5	100.13%±0.76%
BF @7.5	102.68%±0.57%	BF @12.5	102.60%±0.57%	BF @17.5	101.63%±0.53%	BF @22.5	102.15%±0.74%	BF @27.5	99.65%±0.75%
BF @8.5	103.12%±0.56%	BF @13.5	102.82%±0.54%	BF @18.5	102.02%±0.76%	BF @23.5	101.09%±0.66%	BF @28.5	99.16%±0.73%
BF @9.5	104.61%±0.58%	BF @14.5	102.97%±0.53%	BF @19.5	102.58%±0.64%	BF @24.5	102.31%±0.79%	BF @29.5	99.04%±0.62%
TF @10.5	25.19%±0.09%	TF @15.5	11.71%±0.16%	TF @20.5	4.25%±0.11%	TF @25.5	1.22%±0.08%	TF @30.5	0.52%±0.11%
DD	1.73%±0.76%	DD	1.33%±0.81%	DD	0.71%±0.90%	DD	0.65%±0.86%	DD	0.09%±0.85%
DIFF	2.00%	DIFF	2.00%	DIFF	1.00%	DIFF	4.00%	DIFF	-1.00%

Table 7 Numerical result A10 / PEEK-Ac

A6 – PEEK-Ac									
Target 10 mm		Target 15 mm		Target 20 mm		Target 25 mm		Target 30 mm	
BF @6.5	101.64%±0.35%	BF @11.5	101.03%±0.45%	BF @16.5	101.08%±0.37%	BF @21.5	99.78%±0.53%	BF @26.5	100.56%±0.49%
BF @7.5	102.15%±0.49%	BF @12.5	101.55%±0.43%	BF @17.5	100.74%±0.43%	BF @22.5	100.44%±0.69%	BF @27.5	100.30%±0.51%
BF @8.5	102.93%±0.41%	BF @13.5	101.28%±0.39%	BF @18.5	100.36%±0.54%	BF @23.5	101.08%±0.52%	BF @28.5	100.83%±0.52%
BF @9.5	103.38%±0.42%	BF @14.5	102.91%±0.43%	BF @19.5	101.38%±0.52%	BF @24.5	100.90%±0.58%	BF @29.5	100.35%±0.58%
TF @10.5	24.98%±0.06	TF @15.5	11.71%±0.13%	TF @20.5	4.28%±0.12%	TF @25.5	1.21%±0.07%	TF @30.5	0.55%±0.11%
DD	1.51%±0.59%	DD	0.85%±0.60%	DD	0.19%±0.69%	DD	-0.14%±0.71%	DD	0.27%±0.71%
DIFF	1.00%	DIFF	4.00%	DIFF	1.50%	DIFF	2.00%	DIFF	4.00%

Table 8 Numerical result A6 / PEEK-Ac

A5 – PEEK-Ac									
Target 10 mm		Target 15 mm		Target 20 mm		Target 25 mm		Target 30 mm	
BF @6.5	101.80%±0.44%	BF @11.5	101.07%±0.45%	BF @16.5	100.56%±0.46%	BF @21.5	99.75%±0.47%	BF @26.5	98.13%±0.52%
BF @7.5	101.85%±0.32%	BF @12.5	101.56%±0.37%	BF @17.5	100.64%±0.46%	BF @22.5	99.34%±0.39%	BF @27.5	99.31%±0.51%
BF @8.5	102.19%±0.38%	BF @13.5	101.96%±0.46%	BF @18.5	101.69%±0.43%	BF @23.5	100.41%±0.46%	BF @28.5	99.43%±0.65%
BF @9.5	102.99%±0.41%	BF @14.5	102.06%±0.38%	BF @19.5	101.65%±0.53%	BF @24.5	100.81%±0.45%	BF @29.5	100.06%±0.43%
TF @10.5	25.87%±0.16%	TF @15.5	12.23%±0.11%	TF @20.5	4.25%±0.11%	TF @25.5	1.20%±0.07%	TF @30.5	1.02%±0.06%
DD	0.99%±0.54%	DD	0.32%±0.65%	DD	-0.02%±0.61%	DD	-0.32%±0.59%	DD	-0.47%±0.66%
DIFF	0.00%	DIFF	-2.00%	DIFF	0.00%	DIFF	3.00%	DIFF	-2.00%

Table 9 Numerical result A5 / PEEK-Ac

Bibliography

[1] Istisan, R., Andreoli, S., Ciabattoni, A., de Angelis, C., Leonardi, M. C., Menegotti, L., Pimpinella, M., & Rosi, A. (2021). Assicurazione di qualità nella radioterapia intraoperatoria Aggiornamento del Rapporto ISTISAN 03/1.

[2]Oggioni R, Pontecorvo C, Raimondi M, Ratto GA Raccomandazioni per i trasferimenti inter e intra ospedalieri SIAARTI, 31 ottobre 2012 Prot. n. 562/b. Napoli http://timeoutintensiva.it/tecne_data/8_1_linee_guida_file_42.pdf

[3] N Jabbari, B Hashemi-Malayeri,ARFarajollahi, A Kazemnejad, A Shafaei and S Jabbari (2007). Comparison of MCNP4C and EGSnrc Monte Carlo codes in depth-dose calculation of low energy clinical electron beams. Journal of Physics D Applied Physics, 40 (2007) 4519–4524.

[4]NCCN. National Comprehensive Cancer Network. Radiation Therapy Compendium. Plymouth Meeting, PA 2020.

[5] Wenz F. Keynote Address at the American Society of Breast Surgeons 18th Annual Meeting: Current and Future Application of Intraoperative Radiotherapy (IORT) in the Curative and Palliative Treatment of Breast Cancer. Ann Surg Oncol 2017;24(10):2811-17.

[6]. Andreoli S, Fortunato M, Moretti R, Personeni A, Gritti G, Källi M. Micromosfet in vivo dosimetry in early-breast cancer IORT: report on three years of practice. Radioth and Oncol 2009; 92(suppl.1):S231.

[7]. Petoukhova A, Rüssela I, Nijst-Brouwersa J, van Wingerdena K, van Egmonda J, Jacobs D, Marinelli A, van der Sijp J, Koper P, Struikmans H. In vivo dosimetry with MOSFETs and GAFCHROMIC films during electron IORT for accelerated partial breast irradiation. Physica Medica 2017; 44:26-33.

[8] H. Alhamadaa, S. Simona,b, C. Philippsonb, C. Vandekerkhoveb, Y. Jouranib, N. Paulya, D. Van Gestelb, N. Reynaertb (2020). Monte Carlo dose calculations of shielding disks with different material combinations in intraoperative electron radiation therapy (IOERT). Cancer/Radiothérapie 24 (2020) 128–134

[9] Hamid Reza Baghani, Mostafa Robatjazi, Seyed Rabi Mahdavi (2020). Comparing the performance of some dedicated radioprotection disks in breast intraoperative electron radiotherapy: a Monte Carlo study. Radiation and Environmental Biophysics (2020) 59:265–281

[10] Mostafa Robatjazia, Hamid Reza Baghanic, Seied Rabi Mahdavicd, Giuseppe Felicie (2018). Evaluation of dosimetric properties of shielding disk used in intraoperative electron radiotherapy: A Monte Carlo study. Applied Radiation and Isotopes 139 (2018) 107–113

[11] Norman R. Williams, Katharine H. Pigott, Chris Brew-Graves, Mohammed R. S. Keshtgar. Intraoperative radiotherapy for breast cancer. Gland Surgery 2014;3(2):109-119.

[12] Lesti Dottssa Sara Raselli, G. (2010). La IORT ad elettroni nel trattamento conservativo dell'Early Breast Cancer A cura della Direzione Scientifica.

[13] Vaidya, J. S., Tobias, J. S., Baum, M., Keshtgar, M., Joseph, D., Wenz, F., Houghton, J., Saunders, C., Corica, T., D'Souza, D., Sainsbury, R., Massarut, S., Taylor, I., & Hilaris, B. (2004). Intraoperative radiotherapy for breast cancer. In Lancet Oncology (Vol. 5, Issue 3, pp. 165–173).

[14] Calvo F, Sole C, Herranz R, Lopez-Bote M, Pascau J, Santos A, Muñoz-Calero A, Ferrer C and Garcia-Sabrido JL. Intraoperative radiotherapy with electrons: fundamentals, results, and innovation. Ecancermedicalscience 2013;7:339.

[15] Fastner G, Gaisberger C, Kaiser J, Scherer P, Ciabattoni A, Petoukhova A, Sperk E, Poortmans P, Calvo FA, Sedlmayer F, Leonardi MC. ESTRO IORT Task Force/ACROP recommendations for intraoperative radiation therapy with electrons (IOERT) in breast cancer. Radioth Oncology. Guidelines 2020;149:150-7.

[16] Avizonis VN, Sause WT, Noyes RD. Morbidity and mortality associated with intraoperative radiotherapy. J Surg Oncol 1989;4:240-5.

[17] Cromack DT, Maher MM, Hoektra H, Kinsella TJ, Sindelar WF. Are complications in an intraoperative radiation therapy more frequent than in conventional treatment? Arch Surg 1989;124(2):229-34.

[18] Delanian S, Lefaix JL, Pradat PF. Radiation-induced neuropathy in cancer survivors. Radiotherapy and Oncology 2012;105:273-82.

[19] Veronesi U, Orecchia R, Maisonneuve P, Viale G, Rotmensz N, Sangalli C, Luini A, Veronesi P, Galimberti V, Zurrida S, Leonardi MC, Lazzari R, Cattani F, Gentilini O, Intra M, Caldarella P, Ballardini B. Intraoperative radiotherapy vs. external radiotherapy for early breast cancer (ELIOT): a randomised controlled equivalence trial. Lancet Oncol 2013;14:1269-77.

[20] Rosenstein BS, Lymberis SC, Formenti SC. Biologic comparison of partial breast irradiation protocols. Int J Radiat Oncol Biol Phys 2004;60(5):1393-404.

[21] ICRU. International Commission on Radiation Units and Measurements. Radiation dosimetry: Electron beams with energy between 1 and 50 MeV. Report 35. Bethesda, Maryland 1984.

[22] Beddar AS, Biggs PJ, Chang S, Ezzel GA, Faddegon BA, Hensley FW, Mills MD. Intraoperative Radiation therapy using mobile electron linear accelerators: Report of AAPM Radiation Therapy Committee Task Group No. 72. Med Phys 2006;33:1476-89.

[23] Gunderson LL, Willett CG, Calvo FA, Harrison LB. (Ed.) Intraoperative Irradiation. Current Clinical Oncology. Techniques and Results. New York, Humana Press, 2011.

[24]. Hensley FW. Present state and issues in IORT Physics. Radiat Oncol 2017;12(37):1-30.

[25]. Bjork P, Nilsson P, Knoos T. Dosimetry characteristics of degraded electron beams investigated by Monte Carlo calculations in a set-up for intraoperative radiation therapy. Phys Med Biol 2002;47:239-256.

[26] Bjork P, Knoos T, Nilsson P. Comparative dosimetry of diode and diamond detectors in electron beams for intraoperative radiation therapy. Med Phys 2000;27:2580-88.

[27] Bjork P, Knoos T, Nilsson P, Larsonn K. Design and dosimetry characteristics of a soft-docking system for intraoperative radiation therapy. Int. J. Radiat Oncol Biol Phys 2000;47:527-33

[28] Bjork P, Knoos T, Nilsson P. Measurements of output factors with different detector types and Monte Carlo calculations of stopping-power ratios for degraded electron beams. Phys Med Biol 2004; 49:4493-4506.

[29] Iaccarino G, Strigari L, D'Andrea M, Bellesi L, Felici G, Ciccotelli A, Benassi M, Soriani A. Monte Carlo simulation of electron beams generated by a 12 MeV dedicated mobile IORT accelerator. Phys. Med. Biol 2011;564:579-96.

[30]. Laitano RF, Guerra AS, Pimpinella M, Caporali C, Petrucci A. Charge collection efficiency in ionization chambers exposed to electron beams with high dose per pulse. Phys Med Biol 2006;51:6419-36.

[31] Piermattei A, delle Canne S, Azario L, Russo A, Fidanzio A, Miceli R, Soriani A, Orvieto A, Fantini M. The saturation loss for plane parallel ionization chambers at high dose per pulse values. Phys Med Biol 2000;45:1869-83.

[32] Di Martino F, Giannelli M, Traino AC, Lazzeri M. Ion recombination correction for very high dose per pulse high-energy electron beams. Med Phys 2005;32:2204-10.

[33] Bruggmoser G, Saum R, Schmachtenberg A, Schmid F, Schule E. Determination of the recombination correction factor kS for some specific plane-parallel and cylindrical ionization chambers in pulsed photon and electron beams. Phys Med Biol 2007;52:N35-N50.

[34] Besheli MG, Simiantonakis I, Zink K, Budach W. Determination of the ion recombination correction factor for intraoperative electron beams. Z Med Phys 2016;26:35-44.

[35] Gotz M, Karsch L, Pawelke J. A new model for volume recombination in plane-parallel chambers in pulsed fields of high dose-per-pulse. Phys Med Biol 2017;62:8634-54

[36] P. Andreo, D. T. Burns, K. Hohlfeld, M. S. Huq Thomas Jefferson, T. Kanai, F. Laitano, V. G. Smyth, S. Vynckier. IAEA TRS-398 "Absorbed Dose Determination in External Beam Radiotherapy: An International Code of Practice for Dosimetry based on Standards of Absorbed Dose to Water".

[37] Spadaro, S. (2013). Scuola Dottorale EDEMOM Sviluppo di Dosimetri in Diamante per Radioterapia.

[38] Rata, R., Panait, R., Butuc, I., Constantin, C., Grivole, M., & Mihailescu, D. (n.d.). Monte Carlo codes for medical radiation physics Related papers Monte Carlo codes for use in medical radiation physics.

[39] Andreo P. (1991), Monte Carlo techniques in medical radiation physics, Phys. Med. Biol. 36, pp. 861-920.

[40] Rogers D. W. O. (2002), "Monte Carlo Techniques in Radiotherapy", Physics in Canada 58, pp. 63-70.

[41] Bielajew, A.F. (2001), "Fundamentals of the Monte Carlo method for neutral and charged particle transport": http://www-personal.umich.edu/~bielajew/.

[42] A. Ferrari, P.R. Sala, A. Fasso`, and J. Ranft. FLUKA: a Multi-Particle Transport Code. CERN 2021-5 (2021).

[44] Reiter, D. (2007). The Monte Carlo Method, an Introduction.

[45] http://rcwww.kek.jp/research/egs/

[46] https://mcnp.lanl.gov/

[47] https://geant4.web.cern.ch/

[48] http://pypenelope.sourceforge.net/

[49] Low, D. A., & Dempsey, J. F. (2003). Evaluation of the gamma dose distribution comparison method. Medical Physics, 30(9), 2455–2464.

[50] Low, D. A., Harms, W. B., Mutic, S., & Purdy, J. A. (1998). A technique for the quantitative evaluation of dose distributions. Medical Physics, 25(5), 656–661.

[51] Righi S, Karaj E, Felici G, Di Martino F. Dosimetric characteristics of electron beams produced by two mobile accelerators, NOVAC7 and LIAC, for intraoperative radiation therapy through Monte Carlo simulation. J of ACMP 2013;14(1):6-18.

[52] Pimpinella M, Mihailescu D, Guerra AS, Laitano RF. Dosimetric characteristics of electron beams produced by a mobile accelerator for IORT. Phys. Med. Biol 2007;52:6197-6214.

[53] Price RA, Ayyangar KM. IORT apparatus design improvement through the evaluation of electron spectral distributions using Monte Carlo methods. Med Phys 2000;27:215-20.

[54] A. Martignano, L. Menegotti, A. Valentini (2007). Monte Carlo investigation of breast intraoperative radiation therapy with metal attenuator plates. Med. Phys. 34 (12), December 2007

[55] Alhamada, H., Simon, S., Philippson, C., Vandekerkhove, C., Jourani, Y., Pauly, N., Dubus, A., & Reynaert, N. (2018). Shielding disk position in intra-operative electron radiotherapy (IOERT): A Monte Carlo study. Physica Medica, 51, 1–6.

[56] Darlington, E. H. (1975). Backscattering of 10-100 keV electrons from thick targets Backscattering of IO-108 keV electrons from thick targets. In J. Phys. D: Appl. Phys (Vol. 8).

[57] Ernest J. Sternglass. (1953). Backscattering of Kilovolt Electron from Solids.

[58] Alhamada, H., Simon, S., Philippson, C., Vandekerkhove, C., Jourani, Y., Pauly, N., VanGestel, D., & Reynaert, N. (2019). 3D Monte Carlo dosimetry of intraoperative electron radiation therapy (IOERT). Physica Medica, 57, 207–214.

[59] Mohamed E. Mahmoud, Ahmed M. El-Khatib, Mohamed S. Badawi, Amal R. Rashed, Rehab M. El-Sharkawy, Abouzeid A. Thabet (2017). Recycled high-density polyethylene plastics added with lead oxide nanoparticles as sustainable radiation shielding materials. Journal of Cleaner Production.

[60] A. El-Sayed Abdoa, M.A.M. Alib, M.R. Ismail (2003). Natural fibre high-density polyethylene and lead oxide composites for radiation shielding. Radiation Physics and Chemistry 66 (2003) 185–195.

[59] Casella, G., Robert, C. P., & Wells, M. T. (2004). Generalized Accept-Reject sampling schemes (pp. 342–347).

[60] Chvetsov, A. v., & Sandison, G. A. (2002). Reconstruction of electron spectra using singular component decomposition. Medical Physics, 29(4), 578–591.

[61] Hohlfeld, K. (2006). Dosimetry and Medical Radiation Physics Section.

[62] M Robatjazi, K Tanha, SR Mahdavi, HR Baghani, HR Mirzaei, M Mousavi, N Nafissi, E Akbari , S. R. (2018). Monte Carlo Simulation of Electron Beams produced by LIAC Intraoperative Radiation Therapy Accelerator. In J Biomed Phys Eng (Vol. 8, Issue 1).

[63] Tho, T. H., & Nguyen-Truong, H. T. (2019). Electron elastic backscattering probability and inelastic mean free path. Journal of Physics Condensed Matter, 31(41).

[64] Wysocka-Rabin, A., Adrich, P., & Wasilewski, A. (2011). Monte Carlo Study of a New Mobile Electron Accelerator Head for Intra Operative Radiation Therapy (IORT). In Progress in NUCLEAR SCIENCE and TECHNOLOGY (Vol. 2).

[65] Wysocka-Rabin, A., Adrich, P., & Wasilewski, A. (2014). Radiation protection studies for a new mobile electron accelerator for intra operative radiation therapy (IORT). Progress in Nuclear Science and Technology, 4, 298–302.

[66] G. F. Knoll, Radiation Detection and measurement. John Wiley and Sons, Inc., 2010.

[67] M Catalano, S Agosteo, R Moretti, S Andreoli (2007). Montecarlo simulation code in optimisation of the IntraOperative Radiation Therapy treatment with mobile dedicated accelerator. Journal of Physics: Conference Series 74, 2007

[68] Sorrentino L, Fissi S, Meaglia I, Bossi D, Caserini O, Mazzucchelli S, Truffi M, Albasini S, Tabarelli P, Ivaldi GB, Corsi F. One-step intraoperative radiotherapy optimizes conservative treatment of breast cancer with advantages in quality of life and work resumption. The Breast 2018;39:123-30.

[69] Baghani HR, Aghamiri SMR, Mahadavi SR, Akbari ME, Mirzaei HR. Comparing the dosimetric characteristics of the electron beam from dedicated intraoperative and conventional radiotherapy accelerators. Journal of ACMP 2015;16:62-72.

[70] Scalchi P, Ciccotelli A, Felici G, Massafra R, Piazzi V, D'Avenia P, Cavagnetto F, Cattani F, Romagnoli R, Soriani A. Use of parallel-plate ionization chambers in reference dosimetry of NOVACand LIAC mobile electron linear accelerators for intraoperative radiotherapy: a multi-center survey. Med Phys 2017;44(1):321-32.

[71] Nevelsky A, Bernstein Z, Bar-Deroma R, Kuten A, Orion I. Design and dosimetry characteristics of a commercial applicator system for intra-operative electron beam therapy utilizing ELEKTA Precise accelerator. J of Applied Clinical Medical Physics 2010;11(4):57-69.

[72] Calamia E, Lucio F, Boriano A, Fillini C, Gerbino A, Dutto A, Chauvie S. In vivo dosimetry on 428 patients with breast cancer treated with intraoperative radiation therapy in presence of different internal shielding in materials. Physica Medica 2016;32(suppl):36-7.

[73] Hirayama, H. and Namito, Y. (2001), "Lecture Notes of Radiation Transport Calculation by Monte Carlo Method" KEK Internal 2000-20, available at: http://rcwww.kek.jp/research/egs/kek/egs4/mcl_en.pdf.

List of Figures

List of Tables